Metabotropic glutamate receptor 4-mediated glutamatergic signaling reshapes the tumor microenvironment by regulating dendritic cell maturation

Xiaoman Ju[1,6], Eva Maria Putz [2,6], Yaqi Liu[1], Dongchen Yuan[1], Guowei Sun[1], Stephane Koda[1], Zhuo Fu[1], Simin Shao[1], Chunrong Tong[3] ✉, Biping Deng [4] ✉, Jing Hu [5] ✉ & Juming Yan [1] ✉

Metabotropic glutamate receptor 4 (mGluR4, encoded by *Grm4*), is a neurotransmitter receptor, known to play roles in tumor progression and immune modulation through the nervous system. Here we show that mGluR4 may regulate immune responses in the tumor microenvironment (TME) also via non-neuronal mechanisms. We observe that dendritic cells (DC) from mGluR4-deficient mice display enhanced migration, maturation and antigen-presentation capacity, which promote T cell and NK cell responses against tumor cells. Tumor growth and metastases are suppressed in *Grm4*^{-/-} mice in different preclinical tumor models, including orthotopic liver cancer, sub-cutaneous melanoma, colorectal tumors, and fibrosarcoma. We show that the tumor suppressive effect of *Grm4*-deficiency requires host immunity, in particular CD8^{+} T cells, NK cells, and IFNγ, but independent of the nervous system. Single-cell RNA-sequencing and ex vivo assays show changes in the composition and functional state of the immune TME. Mechanistically, mGluR4 suppresses the adenyl cyclase/PKA signaling pathway, leading to metabolic reprogramming of DCs. Importantly, adoptive transfer of DCs pretreated with the AC agonist forskolin therapeutically suppressed tumor growth in an orthotopic liver cancer model. Our study thus demonstrates that mGluR4 is a checkpoint for DC maturation and that mGluR4 may serve as an immunotherapeutic target.

Dendritic cells (DC) orchestrate antitumor immunity and immunotherapy[1]. DCs are the most potent professional antigen-presenting cells (APCs), which can uptake, process, and present various antigens to naïve T cells. DCs promote immunity or tolerance by sampling and presenting antigens to T cells and by providing immunomodulatory signals through cell-cell contacts and cytokines[2,3]. DCs can regulate the activation of potent antitumor T cells and immune responses. However, the immunosuppressive

[1]Department of Pathogen Biology and Immunology, Jiangsu Key Laboratory of Immunity and Metabolism, Jiangsu International Laboratory of Immunity and Metabolism, Xuzhou Medical University, Xuzhou, Jiangsu, China. [2]Center for Physiology and Pharmacology, Institute of Pharmacology, Medical University of Vienna, Vienna, Austria. [3]Department of Hematology, Beijing GoBroad Boren Hospital, Beijing, China. [4]Cytology Laboratory, Beijing GoBroad Boren Hospital, Beijing, China. [5]Department of Bioinformatics; Department of Genetics, Xuzhou Engineering Research Center of Medical Genetics and Transformation, Xuzhou Medical University, Xuzhou, Jiangsu, China. [6]These authors contributed equally: Xiaoman Ju, Eva Maria Putz.
✉e-mail: tongcr@gobroadhealthcare.com; dengbp@gobroadhealthcare.com; jhu@xzhmu.edu.com; jumingyan@xzhmu.edu.cn

tumor microenvironment (TME) can affect DC effector functions, altering DC phenotype and promoting dysfunction and tolerogenicity.

DCs mediate immune tolerance through various mechanisms in the TME. Immature DCs express only low levels of the costimulatory molecules CD80, CD86, and MHC[4]. Presentation of antigens without costimulatory signals leads to T cell anergy[5]. Cytokines from DCs are critical for directing immune responses. The production of IL-12 and interferons by DCs promotes cytotoxic T-cell and Th1 cell-dominated immunity[6]. However, tumor-infiltrating DCs produce high levels of inhibitory cytokines, including IL-10 and TGFβ, and chemokines such as CCL2 to recruit tumor-promoting myeloid cell,s including tumor-associated macrophages (TAMs). In addition, DCs modulate anti-tumor immunity by modifying the availability of nutrients. The enzyme indoleamine 2,3-dioxygenase 1 (IDO1) and arginase expressed in DCs deplete the essential amino acids L-tryptophan and arginine in T cells and generate immune suppressive metabolites[7]. Furthermore, DCs limit T cell activation and function through the engagement of inhibitory receptors, such as PD-L1[8].

The functions of DCs are determined by their integration of environmental signals. DCs scan the local environment through their membrane and cytosolic receptors that recognize different types of danger signals[9]. Accumulating evidence substantiates that neural signals play an important role in regulating the immune responses in the TME[10-16]. Glutamatergic signaling, critical for normal nervous system function, modulates innate immunity through receptors expressed in immune cells[17-21]. There are two types of glutamate receptors, ionotropic receptors (iGluRs) (ligand-gated cation channels) and metabotropic glutamate receptors (mGluRs)[22]. The mGluRs belong to the group C family of G protein-coupled receptors, and are composed of eight members, mGluR1 to mGluR8, and are divided into three groups. mGluRs are activated by glutamate and coupled with intracellular G proteins to mediate intracellular second messenger signaling, which is involved in the regulation of neuronal excitation and synaptic transmission. mGluR4 (Encoded by *Grm4*) belongs to group III and is coupled to Gi and Go proteins, and is a presynaptic glutamate receptor, which is expressed in the basal ganglia circuit that controls movement and participates in the neurotransmission of presynaptic excitatory glutamate signals. The role of mGluR4-mediated glutamatergic signaling in regulating immune responses was first reported by Fallarino and colleagues in autoimmune disorders in the central nervous system (CNS)[17]. Mice lacking mGluR4 were shown to be highly susceptible to experimental autoimmune encephalomyelitis (EAE, a mouse model of multiple sclerosis). Deficiency of mGluR4 altered the profile of cytokine production in DCs, leading to EAE progression[17].

A previous study found that mGluR4 deficiency in mice accelerated radiation-induced murine osteosarcoma development, which was associated with the elevated level of cytokine IL-23[18]. GRM4 gene polymorphism is associated with increased susceptibility and clinicopathological characteristics of osteosarcoma[23,24]. On the contrary, many studies reported that mGluR4 expression in human tumor cells directly promoted proliferation, survival and invasion as well as xenograft tumor growth[25]. mGluR4 promoted tumor growth in murine syngeneic subcutaneous tumor models[26]. This indicates that the role of mGluR4 in regulating immune responses varies in different tumor settings. However, the mechanism of mGluR4-mediated glutamatergic signaling in regulating immune responses to tumors remains largely unknown.

Here, we demonstrate that mGluR4 operates beyond neuronal contexts to suppress DC functionality, establishing a tumor-intrinsic mechanism of immune evasion. Genetic or pharmacological inhibition of mGluR4 enhances DC maturation, antigen presentation, and anti-tumor immunity across diverse preclinical models. These effects rely critically on adaptive and innate immune components, including CD8+ T cells, NK cells, and IFNγ signaling. Our findings position mGluR4 as a

druggable checkpoint governing DC-mediated antitumor responses, with broader implications for targeting metabolic signaling pathways to overcome immunosuppression in cancer and other immune-driven pathologies.

Results

mGluR4 suppresses the maturation and function of DCs

The expression of mGluR4 in myeloid cells has been reported previously[17,18,26]. We confirmed the presence of *Grm4* mRNA in different myeloid cell subtypes and observed the highest *Grm4* levels in bone marrow-derived dendritic cells (BMDCs) (Fig. 1A). In the TME, tumor cell-derived factors impact gene expression and function of DCs. We found that tumor cell-conditioned media (TCM) substantially upregulated the gene expression of *Grm4* in BMDCs (Fig. 1B). Loss of mGluR4 in mice increased the levels of proinflammatory cytokines in BMDCs including TNFα, IL-6, IL-12 and IL-23 (Supplementary Fig. 1A, B), indicating the important role of mGluR4-mediated glutamatergic signaling in DCs. Moreover, our results indicate that mGluR4-deficient DCs expressed significantly higher levels of co-stimulatory molecules CD40, CD80, and CD86 compared to wild-type (WT) DCs in the presence of TCM (Fig. 1C, D).

The maturation status of DCs correlates with their potential to initiate adaptive immune responses[27]. Next, we set up a DC and CD8+ T cell co-culture assay to assess the effect of mGluR4 on the function of DCs as shown in Fig. 1E. Compared to WT DCs, *Grm4*-/- DCs were significantly more potent in inducing proliferation and IFNγ production of CD8+ T cells (Fig. 1F, G). Pre-treatment of DCs with TCM generally suppressed the ability of DCs to promote the proliferation and cytokine production of CD8+ T cells compared with FM (Fig. 1F–H), which mimicked the impact of TME on DCs. The proportions of IFNγ+ and Granzyme B+ CD8+ T cells were increased when co-cultured with *Grm4*-/- DCs pre-treated with FM and TCM settings (Fig. 1H). When WT and *Grm4*-/- DCs were co-cultured with WT CD4+ T cells, similar results were obtained as with CD8+ T cells (Supplementary Fig. 1C, D). Furthermore, CD8+ T cells displayed higher cytotoxicity against tumor cells after co-culture with *Grm4*-/- DCs compared with WT DCs (Fig. 1I).

The regulatory effect of mGluR4 on DCs was further confirmed in vitro using an immortalized dendritic cell line. Knocking out *Grm4* in the murine DC cell line DC2.4 (*Grm4* KO-DC2.4) by CRISPR-Cas9 generated a cytokine expression profile associated with DC activation (Supplementary Fig. 2A, B) and increased co-stimulatory molecule expression compared to the control-DC2.4 cells (Supplementary Fig. 2C). Functionally, OVA antigen-loaded *Grm4* KO-DC2.4 cells were more capable of promoting CD8+ T cell proliferation compared to control-DC2.4 cells (Supplementary Fig. 2D). Conversely, over-expression of *Grm4* in DC2.4 cells (*Grm4* OE-DC2.4) significantly downregulated the levels of TNFα, IL-6, IL-12, and co-stimulatory molecules and decreased the antigen presentation ability as determined by CD8+ T cell proliferation (Supplementary Fig. 2E–G).

Furthermore, treatment with ADX88178, a potent mGluR4 positive allosteric modulator, reduced the production of proinflammatory cytokine TNFα, IL-6, and IL-12, and co-stimulatory molecule expression and impaired proliferation of CD8+ T cells (Supplementary Fig. 3A–C). In contrast, UBP1112, a selective group III mGluR antagonist, promoted the maturity and function of DCs (Supplementary Fig. 3A, D, E). These complementary findings reinforce the conclusion that mGluR4 signaling in DCs plays a critical role in modulating T cell responses.

In contrast to DCs, BMDMs expressed only low levels of *Grm4* (Fig. 1A). Consistent with the low expression of *Grm4* in BMDMs, we did not observe any functional impact of mGluR4 on BMDMs (Supplementary Fig. 4A–C). *Grm4* is expressed in various immune cells at the mRNA level[17,18,26]. Although we confirmed the mRNA levels of *Grm4* in different immune cell subtypes (Supplementary Fig. 5A), no significant differences in the proliferation of CD4+ and CD8+ T cells from WT and *Grm4*-/- mice were observed (Supplementary Fig. 5B). In addition, the
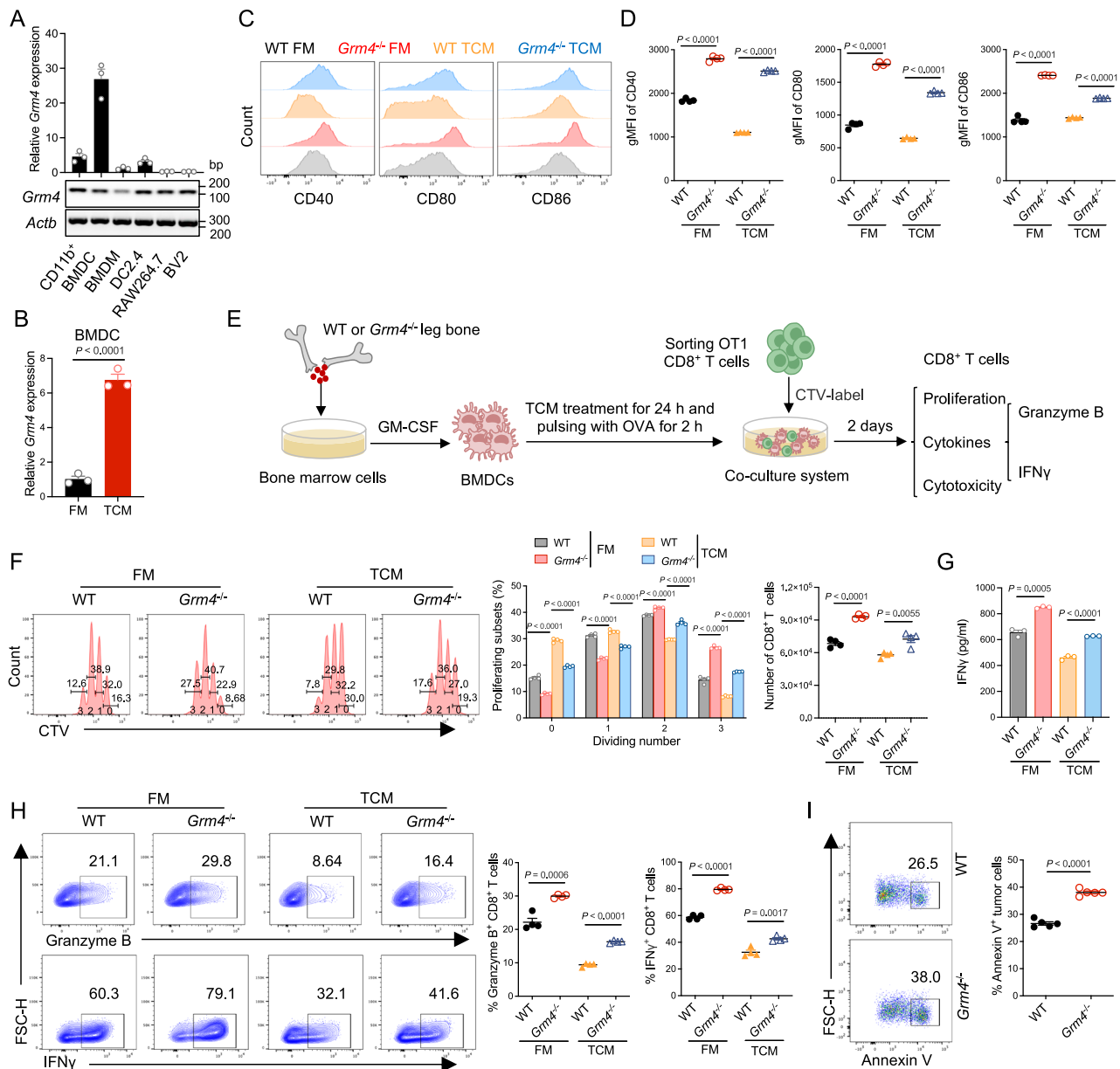
Fig. 1 | mGluR4 suppresses the maturation and function of DCs. A The CD11b⁺ cells were purified from spleens of WT mice, and BMDCs and BMDMs were induced by GM-CSF (20 ng/ml) or L929 cellular supernatant, respectively ($n = 3$ biological replicates). The RNA levels of mGluR4 were analyzed by qPCR analysis. **B** BMDCs pretreated with fresh media (FM) or Hepa1-6BL tumor cell conditioned media (TCM) for 24 h ($n = 3$ biological replicates). The expression of *Grm4* was determined by qPCR. **C** Expression level of CD40, CD80, and CD86 in WT or *Grm4⁻/⁻* BMDCs cultured with FM or Hepa1-6BL TCM for 24 h. **D** Geometric mean fluorescence intensity (gMFI) of CD40, CD80, and CD86 in WT or *Grm4⁻/⁻* BMDCs from (**C**) ($n = 4$ biological replicates). **E** Diagram of CD8⁺ T cell and BMDC coculture assay. **F–I** WT or *Grm4⁻/⁻* BMDCs were cultured in FM or Hepa1-6BL TCM for 24 h, then pulsed with 1 ng/ml OVA peptide for 2 h before being co-cultured with CTV-labeled OT1 CD8⁺

T cells in a 1:10 ratio. T-cell proliferation, cytokine production, and cytotoxicity against tumor cells were measured 2 days later. **F** Representative histogram plots and statistical analysis of the proliferation of CD8⁺ T cells (The clusters of 1, 2, and 3 represent the different times of division of CD8⁺ T cells, respectively, and 0 represents the initial CD8⁺ T cells) ($n = 4$ biological replicates). **G** The level of IFNγ in the cell culture supernatant from (**F**) was measured by ELISA kit ($n = 3$ biological replicates). **H** Expression levels of granzyme B and IFNγ in CD8⁺ T cells ($n = 4$ biological replicates). **I** The apoptosis of Hepa1-6BL ($n = 5$ biological replicates). Data were presented as mean ± SEM. Statistical significance was determined by unpaired *t*-test two-tailed (**B, D, F, G, H, I**). All biological experiments were repeated at least three times and yielded consistent results. Source data are provided as a Source Data file.

proportions of IFNγ-producing CD4⁺, and CD8⁺ T cells were similar between WT and *Grm4⁻/⁻* mice (Supplementary Fig. 5C, D). In summary, our data suggests that mGluR4 has no major direct impact on the proliferation or function of the above immune cells.

Deficiency of mGluR4 delays tumor progression and prolongs mouse survival

Given the importance of DCs in regulating anti-tumor immune responses and the role of mGluR4 in regulating DC maturation, we

determined the effect of mGluR4 on tumor growth and metastases in different syngeneic tumor models. For the orthotopic liver tumor model, Hepa1-6BL cells were rapidly inoculated via hydrodynamic tail vein injection. This model mimics the human liver tumor microenvironment and is characterized by spontaneous metastasis to the lung, a common site of metastasis in liver cancer patients. The liver tumor burden was markedly decreased in *Grm4⁻/⁻* mice compared with WT mice, including the weight of tumor-bearing livers, the total number of liver tumor foci, and the number of tumors with different

sizes (Fig. 2A, B). Hepa1-6BL tumor-bearing $Grm4^{-/-}$ mice developed fewer lung metastases and lower serum levels of AST and ALT than WT mice (Fig. 2C, D). Consequently, the survival of Hepa1-6BL tumor-bearing $Grm4^{-/-}$ mice was significantly prolonged compared with WT mice (Fig. 2E). The growth of subcutaneous Hepa1-6BL liver tumor, MC38-OVA^{dim} colorectal tumor, SM1WT1 melanoma and MCA1956 fibrosarcoma were significantly suppressed, and the tumor mass was decreased in $Grm4^{-/-}$ mice compared with WT mice and some cure achieved (Fig. 2F–J). Loss of mGluR4 also substantially decreased the experimental lung metastasis number of MC38 colorectal tumors and B16F10 melanoma by about 50% (Fig. 2K, L). These results demonstrate that the presence of mGluR4 can promote tumor growth and metastases.

mGluR4, best known for its roles in neurons, also has an important immune-modulatory role in the CNS. To further demonstrate whether mGluR4 promoted tumor progression through regulating immune responses rather than the nervous system, we generated four-way bone marrow (BM) chimeric mice from WT or $Grm4^{-/-}$ donors (Fig. 2M). Only mice reconstituted with $Grm4^{-/-}$ BM displayed reduced tumor growth (Fig. 2M), suggesting that mGluR4 promoted tumor progression via suppressing anti-tumor immunity. IFNγ, CD8$^+$ T and NK cells are the major effector molecules and cytotoxic immune cells in controlling solid tumor progression, respectively. mGluR4 deficient mice failed to suppress SM1WT1 tumor growth after neutralization of IFNγ or depletion of CD8$^+$ T or NK cells (Fig. 2N–P), indicating that IFNγ, CD8$^+$ T and NK cells were required for tumor control in mGluR4 deficient mice. Together, these results indicate that independent of the neuron system, mGluR4 deficiency augments anti-tumor immunity and leads to better tumor control.

Previously, our in vitro assay showed that mGluR4 has no direct effect on the proliferation and cytokine production of T cells. To test whether tumor suppression in $Grm4^{-/-}$ mice was attributed to a direct impact of mGluR4 on T cells in vivo, we sorted T cells (CD45.2$^+$TCRβ$^+$) from naïve WT and $Grm4^{-/-}$ mice and transferred them into tumor-bearing $Rag2^{-/-}$ mice lacking endogenous T cells (Supplementary Fig. 6A). There was no difference in the orthotopic liver tumor growth between the groups transferred with WT and $Grm4^{-/-}$ T cells (Supplementary Figs. 6B, C). Together, these results suggest that mGluR4 indirectly regulates T cell-mediated tumor control.

Deficiency of mGluR4 alters the landscape of the TME and the profile of DCs

To evaluate the impact of mGluR4 on the tumor immune microenvironment, we assessed the immune cells infiltrating solid Hepa1-6BL tumors by flow cytometry. The results showed a significant increase in the frequency and number of CD45.2$^+$ cells in tumors growing in $Grm4^{-/-}$ compared to WT mice (Fig. 3A). To gain a comprehensive understanding of the effect of mGluR4 on the liver TME, intratumoral CD45.2$^+$ immune cells were sorted from five tumors that had been growing in $Grm4^{-/-}$ or WT mice and performed single-cell RNA sequencing (scRNA-seq) using the 10× Genomics Chromium platform paired with deep sequencing (Fig. 3B). Tumor-infiltrating CD45.2$^+$ cells were assigned to 13 clusters, based on immune cell marker gene expression (Fig. 3C and Supplementary Figs. 7, 8). The percentage of CD8$^+$ T cells (cluster 1 and 9) and NK cells (cluster 2) increased dramatically, while the frequency of tumor-associated macrophages (TAMs) (clusters 0, 3, and 4) and monocytes (cluster 6) decreased significantly in $Grm4^{-/-}$ mice (Fig. 3D).

Given that our in vitro results showed that mGluR4 intrinsically regulated the maturation and function of DCs, we further analyzed the DCs in the TME. Intratumoral DCs consisted of two clusters: cluster 8 defined as ISG cDC2, is characterized by $Fcer1a$, $Cd1c$, and an interferon signature represented by high expression of genes including $Ifitm1$ and $Ifitm2$, and cluster 12 defined as cDC1, characterized by $Clec9a$ and high

expression of the activating DC markers $Ccr7$ and $Fscn1$ (Supplementary Fig. 7). Gene set enrichment analysis (GSEA) indicated that pathways linked to inflammation and antigen presentation were significantly increased, while reactive oxygen species (ROS) production was downregulated in both mGluR4-deficient tumor-infiltrating DC clusters (Fig. 3E, F). In addition, $Grm4^{-/-}$ DCs of both clusters expressed significantly higher levels of cytokines and chemokines, interferon-responsive genes, and genes associated with DC maturation and antigen presentation (Fig. 3G). Flow cytometric analysis showed a substantially increased recruitment of DCs into tumors grown in $Grm4^{-/-}$ compared with WT mice (Fig. 3H and Supplementary Fig. 9A). In line with the sc-RNA seq data, the frequency of DCs expressing the maturation makers CD80 and CD86 were increased 1.5-2 times in the tumors growing in $Grm4^{-/-}$ mice as determined by flow cytometry (Fig. 3I). Similarly, we found that the infiltration and maturation of DCs in Hepa1-6BL orthotopic liver tumors were increased in $Grm4^{-/-}$ mice (Supplementary Figs. 9B–D).

We next performed an ex vivo analysis of DCs isolated from Hepa1-6BL orthotopic liver tumors and inguinal lymph nodes (iLNs) that were co-cultured with CD8$^+$ T cells for 2 days (Fig. 3J). We observed that tumor-infiltrating $Grm4^{-/-}$ DCs induced higher proliferation and granzyme B and IFNγ production in CD8$^+$ T cells compared with WT DCs (Fig. 3K, L and Supplementary Fig. 9E–G). In addition, tumor-infiltrating $Grm4^{-/-}$ DCs enhanced the cytotoxicity of CD8$^+$ T cells against Hepa1-6BL tumor cells (Fig. 3M and Supplementary Fig. 9H), suggesting that mGluR4 deficiency in DCs led to activation of the adaptive immunity in the TME. To gain further insights into the effects of $Grm4$ on different DC subsets, including type 1 conventional dendritic cells (cDC1), and type 2 cDC (cDC2), we next determined the abundance of different DC subpopulations in the tumor and draining lymph node (dLN). We found that the frequencies and numbers of both cDC1 and cDC2 significantly increased in the tumors and dLNs of $Grm4^{-/-}$ mice (Fig. 3N, O and Supplementary Fig. 9I, J).

Considering the direct regulatory effect of mGluR4 on DCs, we tested whether mGluR4 affects DC development and homeostasis in naïve mice by flow cytometric analysis according to previous studies[28]. The results showed that the frequencies and numbers of cDC1, cDC2, and pDC subsets were highly similar in the BM, iLN, thymus, spleen, liver, and lung, except for an increase in the number of cDC2 in the spleens and livers of $Grm4^{-/-}$ mice (Supplementary Fig. 10A, B). Stimulation of bone marrow cells with FLT3L generates a mixed population of cDC1, cDC2, and pDC cells[28,29]. In line with the in vivo data, BM cells cultured in FLT3L showed a similar ability to differentiate into cDC1, cDC2, and pDC cells (Supplementary Fig. 10C). mGluR4 impacted on the maturation and antigen presentation ability of cDC1, rather than cDC2 or pDC cells (Supplementary Fig. 10D, E), although all three DC subsets expressed a similar amount of $Grm4$ mRNA (Supplementary Fig. 10F).

Given the frequency of TAMs was markedly reduced in $Grm4^{-/-}$ mice (Fig. 3D), further analysis was performed to assess potential functional alterations. GSEA analysis indicated activation of pathways linked to antigen presentation and a down-regulation of ROS production in three tumor-infiltrating macrophage clusters in mGluR4 deficient mice (Supplementary Fig. 11A–C). Similarly, we analyzed TAMs in Hepa1-6BL subcutaneous and orthotopic liver tumors by flow cytometry. In line with the scRNA-seq data, the frequency of TAMs was significantly decreased (Supplementary Fig. 11D–F). However, the co-stimulatory molecules (CD80 and CD86) and MHC II expressing TAMs were significantly increased in $Grm4^{-/-}$ mouse tumor tissues (Supplementary Fig. 11E, F). Despite the changes in TAMs, it is reasonable to suggest that it is an indirect effect, considering our previous findings that macrophages expressed very low levels of $Grm4$ and did not show any functional differences upon loss of mGluR4 (Fig. 1A and Supplementary Fig. 4).
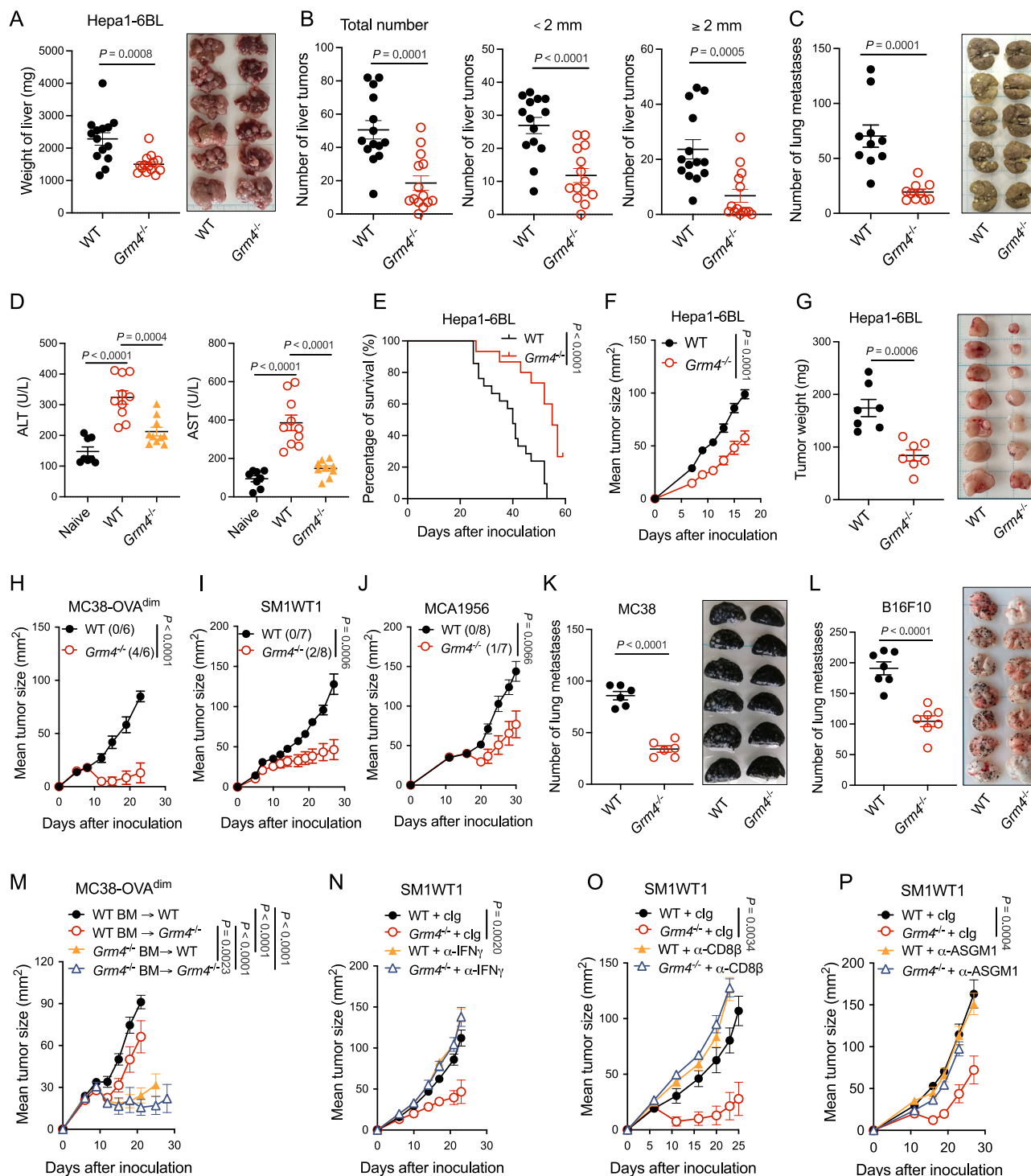
Fig. 2 | Deficiency of mGluR4 delays tumor progression and prolongs mouse survival. A The orthotopic liver tumor surveillance of Hepa1-6BL in WT and *Grm4⁻/⁻* mice was quantified by tumor-bearing liver weight ($n = 14$), **B** the number of liver tumor nodules ($n = 14$), **C** spontaneous lung metastases ($n = 10$), **D** the level of ALT and AST in serum (Naïve $n = 8$, WT $n = 10$, *Grm4⁻/⁻* $n = 10$), **E** and survival of mice (WT $n = 21$, *Grm4⁻/⁻* $n = 15$). **F** Subcutaneous tumor growth, (**G**) weight statistics of Hepa1-6BL in WT and *Grm4⁻/⁻* mice on day 16 ($n = 7$). **H–J** Subcutaneous tumor growth of (**H**) MC38-OVA^dim (WT $n = 6$), (**I**) SM1WT1 (WT $n = 7$, *Grm4⁻/⁻* $n = 8$) and (**J**) MCA1956 (WT $n = 8$, *Grm4⁻/⁻* $n = 7$) cells in WT and *Grm4⁻/⁻* mice (Statistics of tumor rejection rate in the groups was shown in parentheses). **K, L** Lung metastases of (**K**) MC38 ($n = 6$) and (**L**) B16F10 ($n = 7$) cells in WT and *Grm4⁻/⁻* mice. **M** MC38-OVA^dim subcutaneous tumor growth in WT and *Grm4⁻/⁻* mice after BM transplantation (WT BM → WT $n = 9$,

WT BM → *Grm4⁻/⁻* $n = 11$, *Grm4⁻/⁻* BM → WT $n = 10$, *Grm4⁻/⁻* BM → *Grm4⁻/⁻* $n = 10$). **N–P** SM1WT1 subcutaneous tumor growth in WT and *Grm4⁻/⁻* mice after treated intraperitoneally with (**N**) cIg/anti-IFNγ (WT cIg $n = 8$, *Grm4⁻/⁻* cIg $n = 6$, WT α-IFNγ $n = 6$, *Grm4⁻/⁻* α-IFNγ $n = 6$), (**O**) cIg/anti-CD8β (WT cIg $n = 7$, *Grm4⁻/⁻* cIg $n = 6$, WT α-CD8β $n = 6$, *Grm4⁻/⁻* α-CD8β $n = 7$), (**P**) cIg/anti-ASGM1 (WT cIg $n = 6$, *Grm4⁻/⁻* cIg $n = 7$, WT α-ASGM1 $n = 6$, *Grm4⁻/⁻* α-ASGM1 $n = 7$). Data is shown as mean ± SEM. Statistical significance was determined by unpaired *t*-test two-tailed (**A–D, G, K, L**), Mann-Whitney test (two-tailed) (**F, H, I, J**), one-way ANOVA (two-tailed) with Tukey's multiple comparisons test (**M–P**) or log-rank Mantel-Cox test (two-sided) (**E**). All biological experiments were repeated at least three times. Source data are provided as a Source Data file.
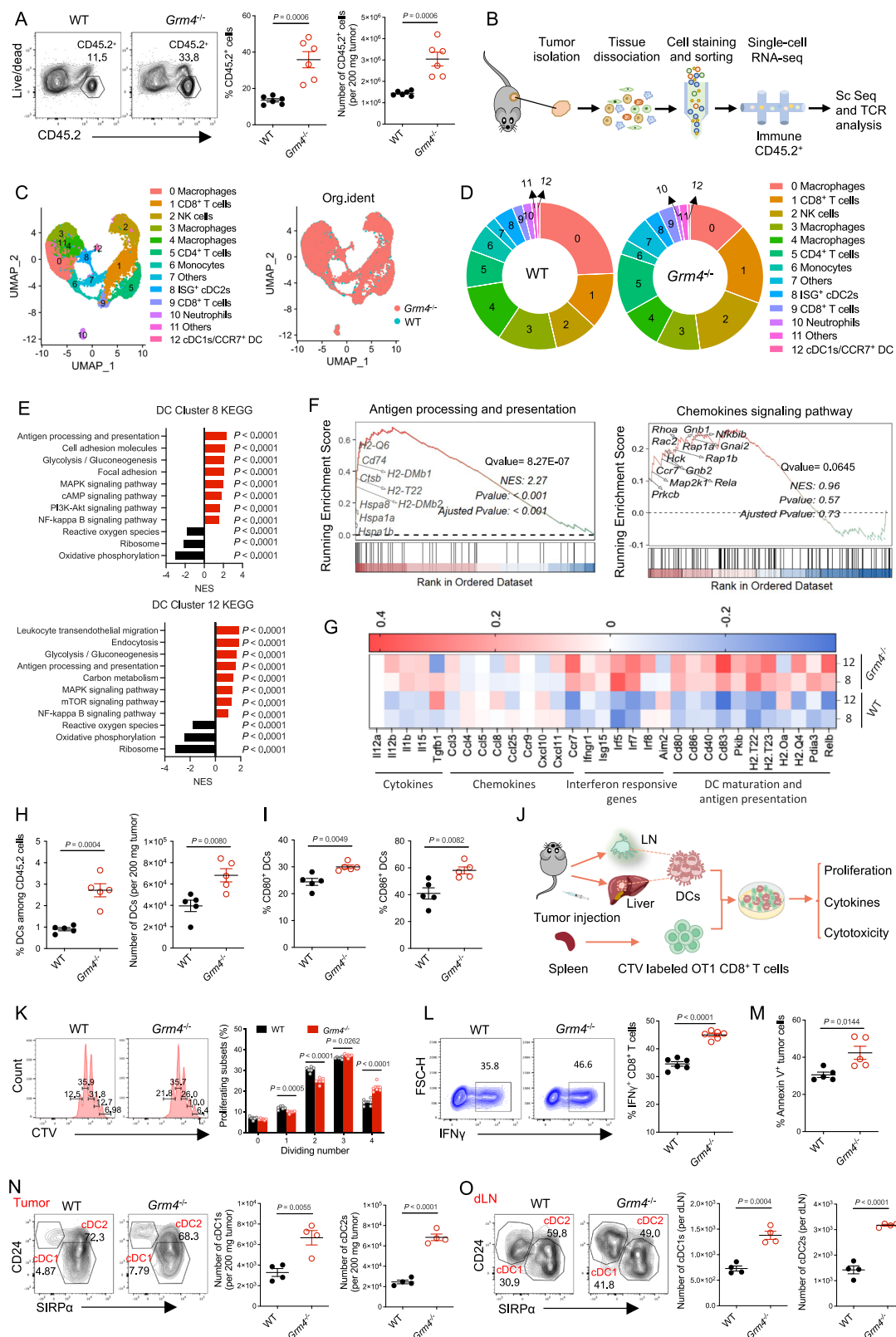
mGluR4 alters the profile of tumor-infiltrating lymphocytes

To study the impact of mGluR4 deficiency on Hepa1-6BL tumor-infiltrating lymphocytes (TILs), we again used the scRNA-seq data and performed GSEA analysis in CD4^{+}, CD8^{+} T cells and NK cells. Overall, we found an upregulation of T cell receptor and cytokine signaling and cell-mediated cytotoxicity in *Grm4^{-/-}* TILs (Fig. 4A). In contrast, cell metabolism such as oxidative phosphorylation (OXPHOS) was

downregulated after loss of mGluR4. Additionally, cell-mediated cytotoxicity-related genes such as *Gzmb* and *Klrc1* were highly upregulated in CD8^{+} T and NK cells isolated from *Grm4^{-/-}* TME compared to WT TME (Fig. 4B, C). Our previous results showed that mGluR4 deficiency did not directly affect the proliferation and function of T cells, but promoted the frequency and function of DCs, which prompted us to investigate the interaction between CD8^{+} T and DCs further. We

Fig. 3 | mGluR4 shapes the immune signature in the TME of the Hepa1-6BL tumors. A Representative plots and quantification of tumor-infiltrating CD45.2^{+} cells in Hepa1-6BL subcutaneous tumors (*n* = 6 mice per group). **B** A schematic diagram illustrating the application of CD45.2^{+} cells, purified from Hepa1-6BL tumors, for single-cell RNA sequencing and TCR analysis. **C** UMAP analysis of CD45.2^{+} cells. **D** Proportions of each cell cluster in the TME of Hepa1-6BL tumors grown in *Grm4^{-/-}* or WT mice. **E** GSEA-KEGG analysis of all DC clusters from Hepa1-6BL tumors. Potential functions and pathway enrichments are shown as normalized enrichment scores (NES) adjusted for multiple comparisons. **F** Visualization of GSEA analysis of core gene variation involved in the function and biological processes of DCs. Statistical testing was performed by permutation test. **G** Heat maps indicate the expression of selected genes in each DC cluster. The statistical difference was calculated by Student's t-test. The P-values were corrected with Benjamini-Hochberg adjustment. **H** Flow cytometry analysis of the frequency and number of tumor-infiltrating DCs among CD45.2^{+} cells in mice bearing Hepa1-6BL subcutaneous tumors (*n* = 5 mice per group). **I** Quantitative plots of CD80 and CD86 in tumor-infiltrating DCs (*n* = 5 mice per group). **J** Schematic diagram of co-culture assay to evaluate the effect of DCs sorted from Hepa1-6BL tumor or LN on OT1 T cell proliferation and effector function. **K** The proliferation of CD8^{+} T cells (*n* = 6 biological replicates), (**L**) quantification of IFNγ expression (*n* = 6 biological replicates), and (**M**) the Annexin V^{+} of tumor cells (*n* = 5 biological replicates). **N, O** Representative flow plot and quantification of CD24^{+} cDC1s and SIRPα^{+} cDC2s in (**N**) tumors and (**O**) draining lymph nodes (dLN) at day 15 after tumor inoculation (*n* = 4 mice per group). Data were presented as mean ± SEM. Statistical significance was determined by unpaired t-test two-tailed (**A, H, I, K, L, M, N, O**) and one-sided (**E, F, G**). All biological experiments were repeated at least three times and yielded consistent results. Source data are provided as a Source Data file.

performed cell-cell interaction analysis and revealed a stronger intercellular connection between DCs and CD8^{+} T cells in the TME of *Grm4^{-/-}* mice compared with WT mice (Fig. 4D). There was a significantly higher interaction score between CD8^{+} T and DCs in *Grm4^{-/-}* mice, in particular, an enriched interaction of antigen presentation related CD28-CD80 and CD28-CD86 and a decreased interaction of inhibitory *Pdcd1* (PD-1)-*Cd274* (PD-L1) (Fig. 4E). This suggested that DCs activated CD8^{+} T cells to produce proinflammatory cytokines and execute direct anti-tumor effector functions. In line, *Grm4^{-/-}* CD4^{+} and CD8^{+} T cells expressed higher levels of the activating receptor DNAM-1, and lower levels of PD-1. Further, *Grm4^{-/-}* CD8^{+} T cells showed a pronounced downregulation of the inhibitory receptors lymphocyte activation gene-3 (LAG3) and T cell immunoglobulin and mucin-domain containing 3 (TIM3) (Fig. 4F), indicating a less exhausted phenotype of T cells in *Grm4^{-/-}* tumors. These results demonstrate that mGluR4 suppresses the function of T cells in the tumor microenvironment via DCs.

Clonality of a T cell response to tumors has been reported to be indicative of the functional state of these cells[30–32]. In addition to the detection of scRNA-seq, we also evaluated the dynamics of the T cell receptor repertoire in the mGluR4-deficient TME by analyzing T cell clonal expansion. We found that the number of unique T cell clones was much higher in *Grm4^{-/-}* than in the WT group (Fig. 4G). The relationship between the number of clonotypes and their abundances indicated that *Grm4^{-/-}* group tumor-infiltrating T cells had a higher clonotype diversity (Fig. 4H). The evenness of the frequency of clone expansions in *Grm4^{-/-}* group tumors was higher than the WT tumors suggesting higher clonotype diversity in T cells in the *Grm4^{-/-}* group (Fig. 4I, J). This indicates that deficiency of mGluR4 in the TME results in an increased diversity of the TCR repertoire.

### mGluR4 deficiency enhances the function of tumor-infiltrating lymphocytes

Our scRNA-seq experiment already suggested a higher number of TILs in the absence of mGluR4. We now used flow cytometry and recapitulated that the frequencies and numbers of CD4^{+}, CD8^{+} T, and NK cells increased more than 2-fold in *Grm4^{-/-}* compared to WT mice bearing s.c. Hepa1-6BL tumors (Fig. 5A and Supplementary Fig. 12A). This was accompanied by a significantly enhanced activity as evidenced by increased IFNγ production and degranulation marker CD107a (Fig. 5B). Like in the s.c. Hepa1-6BL tumor model, also in the orthotopic model, deficiency of mGluR4 markedly increased the infiltration and IFNγ production of CD4^{+} and CD8^{+} T and NK cells (Supplementary Fig. 12B–D). The tumor growth of s.c. and orthotopic tumors is mainly controlled by CD8^{+} T and NK cells[19], while B16F10 experimental lung metastases are essentially contained by NK cells[33,34]. Therefore, the main immune profile in the lungs was determined in the experimental lung metastasis model, to generalize the influence of mGluR4 on TMEs, given that B16F10 experimental lung metastases were suppressed in *Grm4^{-/-}* mice. However, a slightly different picture was observed in B16F10-bearing lungs (Supplementary Fig. 12E–H). The proportion of CD45.2^{+} cells and NK cells was significantly higher in *Grm4^{-/-}* compared with WT mice, however, the number and proportion of CD4^{+} and CD8^{+} T cells remained similar between the two groups (Supplementary Fig. 12E, F). Functionally, a two-fold increase of IFNγ production and CD107a was only observed in NK cells from tumor-bearing lungs of *Grm4^{-/-}* mice compared with WT mice (Supplementary Fig. 12G, H). It indicates that mGluR4 has different impacts on immune cells depending on the tumor model, which could potentially be related to the variable susceptibilities towards the respective effector cells.

Of note, the spleens were much bigger in *Grm4^{-/-}* compared with WT mice in both Hepa1-6BL s.c. and orthotopic tumor models (Fig. 5C and Supplementary Fig. 12I). Flow cytometric analysis showed that the number of CD45.2^{+} lymphocytes, in particular, CD4^{+} and CD8^{+} T cells, was significantly increased in the spleens of *Grm4^{-/-}* mice (Fig. 5D, E). However, the number of NK cells remained similar in the spleens in *Grm4^{-/-}* and WT mice bearing Hepa1-6BL s.c. tumors (Fig. 5E). Further analysis showed that IFNγ, TNFα production, and degranulation (CD107a) were markedly enhanced in tumor-infiltrating T cells and NK cells of *Grm4^{-/-}* mice, with about a two-fold increase (Fig. 5F).

Of interest, we observed an increased number of total immune cells, in particular of CD4^{+}, CD8^{+} T, and NK cells, and also in the dLNs of s.c. Hepa1-6BL-bearing *Grm4^{-/-}* mice, which were also characterized by enhanced IFNγ and TNFα production and degranulation marker (CD107a) (Fig. 5G–I). During the tumor immune cycle, T cells get activated by antigens presented by DCs and expand in the dLN[35]. The observed changes in lymphocyte number and function in the dLNs could thus be explained by the improved function of *Grm4^{-/-}* DCs.

Glutamate is the main ligand of mGluR4[36,37]. The source of glutamate remains unclear in the TME. Previous reports have shown that tumor cells released high levels of glutamate, leading to the activation of the ionotropic glutamate receptor NMDAR (N-methyl-d-aspartate receptors) on TAMs and thereby increasing their immunosuppressive functions[19]. In tumor tissues, a high level of glutamate was observed in MC38 and B16 tumor models[29]. Therefore, we collected tumor interstitial fluid (TIF) and matched plasma and serum from the mice bearing orthotopic liver tumors and determined the level of glutamate. The results showed that glutamate was 4 times higher in TIF and tumor tissue lysate than in the matched plasma and serum (Supplementary Fig. 13A). To further refine the source of glutamate, we examined the cell culture supernatant and cell lysate of tumor cells, DCs, and BMDMs, and found that glutamate levels in TCM and tumor cell lysate were significantly higher than those in BMDC conditioned medium (BMDC CM), BMDC lysate, BMDM conditioned medium (BMDM CM) and FM (Supplementary Fig. 13B). Next, we added sodium glutamate to treat BMDCs in vitro to determine the direct effects of glutamate on DC functions. Like the effect of TCM (Fig. 1C–I) on DCs, glutamate treatment inhibited the expression of BMDC co-stimulatory molecules CD40, CD80, and CD86, and decreased OTI CD8^{+} T cell proliferation and IFNγ production (Supplementary Figs. 13C–E). These results

Figure panels A–J.
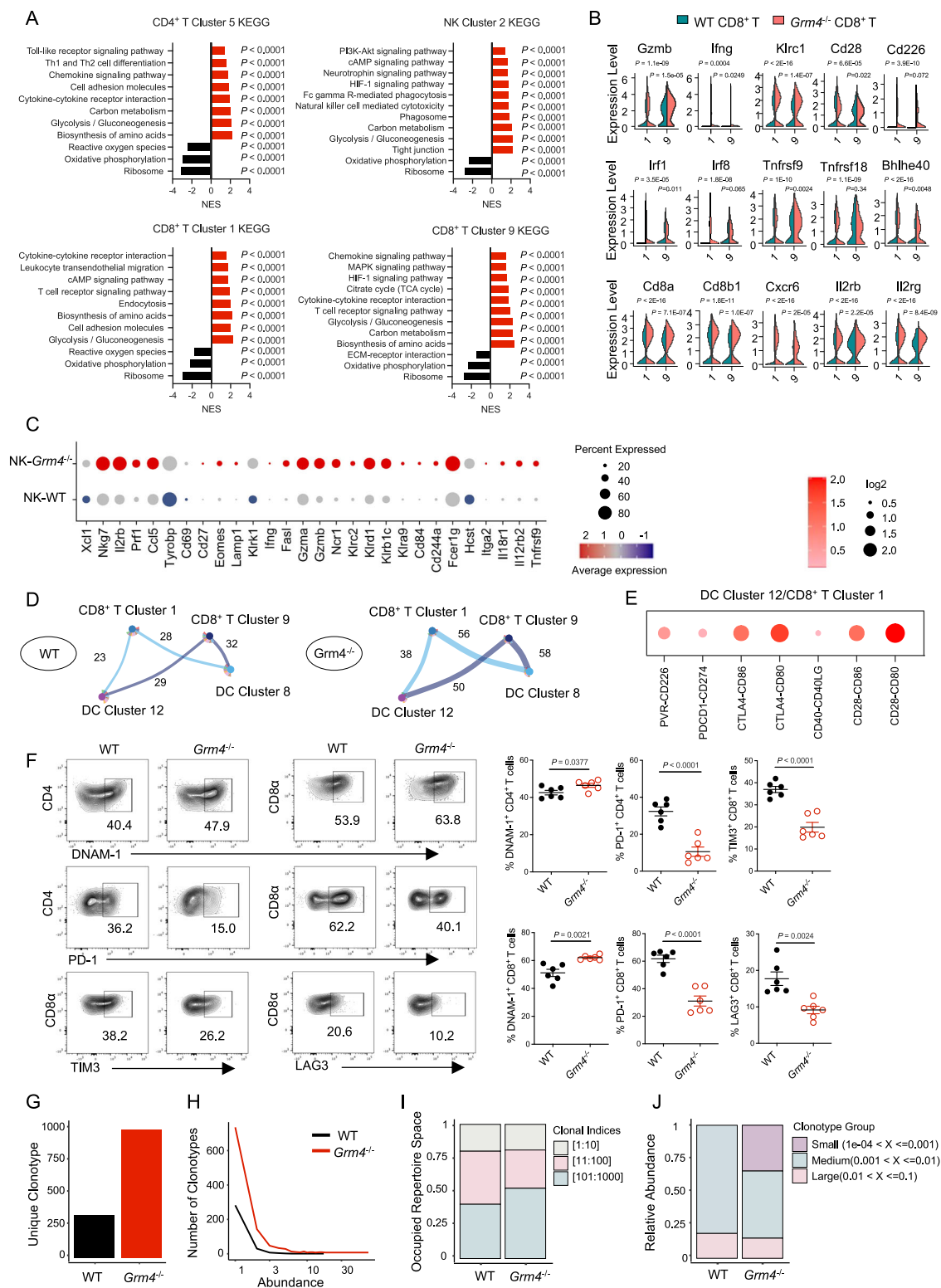
indicate that tumor cell-released glutamate directly impacts on the maturation and function of DCs.

mGluR4 regulates DC metabolism in the TME

To decipher how mGluR4 deficiency impacts the maturation of DCs, we evaluated the effect of mGluR4 on the metabolism of tumor-infiltrating DCs, inspired by recent studies showing that cell metabolism has an important function in supporting DC activation[38–40]. Our scRNA-seq results showed that metabolic pathways such as glucose and carbohydrate catabolic processes, NADPH regeneration, and pyruvate metabolism were amongst the top enriched pathways in DCs of the *Grm4⁻/⁻* group (Supplementary Fig. 14A). The results of GSEA demonstrated that the loss of mGluR4 in Hepa1-6BL-bearing mice led to a simultaneous upregulation of genes associated with glycolysis (e.g., *Gapdh*, *Pkm*, and *Ldha*) and a downregulation of genes involved in oxidative phosphorylation (e.g., *AtpSh*, *Uqcrb*, and *Ndufa2*)

Fig. 4 | mGluR4 alters the profile of tumor-infiltrating lymphocytes. A KEGG pathway enrichment of tumor-infiltrating CD4^{+}, CD8^{+} T, and NK cells from GSEA analysis. **B** Violin diagrams and (**C**) dot plots showing differentially expressed genes in Hepa1-6BL tumor infiltrating CD8^{+} T and NK cells, respectively. **D** The communication analysis between different DC and CD8^{+} T cell clusters by calculating the receptor-ligand interactions. **E** Dot plots of selected ligand-receptor interacting pairs between clusters 8 DCs and clusters 1 CD8^{+} T cells computed using CellPhoneDB. Point shade reflects the log2 Mean of average expression levels of interacting molecule 1 from cluster 1 and interacting molecule 2 from cluster 2. Point size indicates the -log10 (p value). **F** Representative contour plots and the proportion of PD-1, DNAM-1, TIM3, and LAG3 expression in Hepa1-6BL tumor infiltrating CD4^{+} and CD8^{+} T cells (*n* = 6 mice per group). **G** The number of unique clones of the nucleotide sequence combination chain in the CDR3 region in tumor-infiltrating T cells. **H** The relative distribution of the number of clonotypes by abundance for T cells. **I** The relative proportion of the number of clones to the total by frequency of occurrence in all T cells. 1:10 means the top 10 clonotypes in each sample. 11:100 means the number of clones ranked from 11 to 100. 101:1000 means the number of clones ranked from 101 to 1000. **J** The relative proportion of clones at specific proportions to the total number of immune receptor sequences. The specific proportion of clonotypes is classified as small from 0.0001 to 0.001, medium from 0.001 to 0.01, and large from 0.01 to 0.1. Data were presented as mean ± SEM. Statistical significance was determined by unpaired *t*-test two-tailed (**F**) and student's *t*-test one-sided corrected with Benjamini-Hochberg adjustment (**A, B**). All biological experiments were repeated at least three times and yielded consistent results. Source data are provided as a Source Data file.

(Supplementary Fig. 14B, C). Next, we performed a Seahorse assay to validate glycolytic changes in *Grm4*^{-/-} BMDCs and found that mGluR4 deficiency increased basal glycolysis, compensatory glycolysis, and post-2-DG (2-deoxyglucose) acidification (Supplementary Fig. 14D). Accelerated oxidative phosphorylation is known to provide ATP driving tumor growth and generating reactive oxygen species (ROS) byproducts. While a low level of ROS can promote DC activation, a high level of ROS will inhibit DC functions[39,41]. Our scRNA-seq analysis suggested that mGluR4-deficient DCs expressed lower levels of genes involved in ROS production (Supplementary Fig. 14E). Flow cytometric analysis ultimately confirmed that mGluR4 deficiency reduced ROS production in BMDCs (Supplementary Fig. 14F). Under pathological conditions, excessive intracellular ROS will damage mitochondria and cause oxidative stress. Meanwhile, ROS can attack mitochondrial DNA and cause oxidative damage, resulting in structural changes such as mitochondrial membrane potential destruction. Compared with fresh medium, TCM significantly reduced the mitochondrial membrane potential of BMDCs, indicating that the mitochondrial membrane was damaged, while mGluR4 deficiency could increase mitochondrial membrane potential (Supplementary Fig. 14G). These results suggest that mGluR4 impairs glycolysis and mitochondrial fitness, driving ROS production, which is in line with the increased functionality of mGluR4-deficient DCs.

mGluR4 suppresses the maturation of DCs by inhibiting the cAMP/PKA/CREB and NF-kB signaling pathways

mGluR4 is a G protein-coupled receptor associated with Gi that inhibits adenylate cyclase (AC) activity and cyclic adenosine monophosphate (cAMP) downstream signaling[26,42]. It has been reported that mGluR4 plays an inhibitory role in signaling pathways, including cAMP/protein kinase A (PKA)[17,43-45], PI3K/Akt and nuclear factor-κB (NF-κB)[20,46]. GSEA analysis of our scRNA-seq data showed that mGluR4 deficiency led to the upregulation of cAMP, PI3K/Akt, and NF-κB signaling pathways in tumor-infiltrating DCs (Fig. 6A), which was accompanied by increased expression of *Rap1a*, *Rela*, *Jun*, *Rac2*, and *Akt1* (Fig. 6B). Transcription factor analysis suggested that mGluR4-deficient DCs showed enhanced activity of *Spib*, *Etv6*, *Vdr*, and *Nfkb2* (Fig. 6C) that play an important role in regulating the development and function of DCs[42,47]. As a GPCR, activation of mGluR4 can affect multiple downstream signaling pathways and biological processes. Based on the analysis in Figs. 3E, 6A, we determined the effect of mGluR4 on the activation's status of the main components in PI3K/Akt, PKA/CREB, and NF-κB signaling pathways. Indeed, mGluR4-deficiency significantly promoted the phosphorylation of CREB, p65, and Akt in the presence or absence of TCM (Fig. 6D). The presence of the AC agonist forskolin, the PI3K inhibitor TG100713, and the NF-κB inhibitor BAY 11-7082 diminished the effects of mGluR4 on the phosphorylation of CREB, p65, and Akt (Fig. 6E, F and Supplementary Fig. 15A, B). These results confirm the involvement of these pathways downstream of mGluR4 in regulating DC functions. CREB1 modulated CCR7-dependent DC migration, which is critical for the initiation of protective immunity and the maintenance of immune homeostasis. mGluR4 deficiency or AC activation by forskolin increased the expression of CCR7 (Fig. 6G). Correspondingly, mGluR4 deficiency promoted BMDC migration both in vivo and in vitro, with the differences between WT and *Grm4*^{-/-} being abolished by the AC agonist forskolin and PKA inhibitor H89 (Fig. 6H, I and Supplementary Fig. 15C). Moreover, flow cytometric analysis revealed that while H89 showed inhibitory effects, the treatment of DCs with forskolin increased the expression of the DC maturation markers and promoted CD8^{+} T cell proliferation, IFNγ production, and cytotoxicity against tumor cells in WT but not in *Grm4*^{-/-} BMDCs, abrogating the differences observed between WT and *Grm4*^{-/-} BMDCs (Fig. 6J–M and Supplementary Fig. 15D–G). In line, treatment with TG100713 and the BAY 11-7082 inhibited the expression of maturation makers and the function of DCs in activating CD8^{+} T cells both in WT and *Grm4*^{-/-} DCs (Supplementary Fig. 15H, I). These data thus suggest that mGluR4 exerts its biological effects mainly via the cAMP/PKA and PI3K/Akt, and NF-κB signaling pathways to restrict DC migration and activity in the TME.

mGluR4 impairs the anti-tumor efficacy of DC-based tumor vaccines

There is ongoing interest in utilizing DC-based vaccination to stimulate a patient's adaptive immune system against tumor antigens, particularly in settings where endogenous tumor-specific T cells may be lacking. Optimal DC maturation is one prerequisite for successful therapeutic vaccination against tumors[48]. Given the suppressive effect of mGluR4 on the maturation and function of DCs, we determined whether mGluR4 deficiency in DCs augments the efficacy of DC-based tumor vaccines. BMDCs were pulsed with Hepa1-6BL tumor cell lysate and then adoptively transferred into orthotopic liver tumor-bearing WT mice as shown in Fig. 7A, B[49,50]. Repeated vaccination with *Grm4*^{-/-} DCs effectively delayed tumor progression as determined by reduced liver weights, fewer liver tumors, and lower serum levels of AST and ALT, while vaccination with WT DCs was less efficient (Fig. 7C, D). The vaccinations with *Grm4*^{-/-} DCs increased the numbers of tumor-infiltrating CD4^{+} and CD8^{+} T and NK cells, and strongly boosted their function as indicated by higher expression of granzyme B and IFNγ (Fig. 7E, F). Similarly, the percentage of CD4^{+} and CD8^{+} T cells in the LNs was substantially increased in mice that had received *Grm4*^{-/-} DC-based vaccinations (Fig. 7G). Interestingly, the number of DCs in the TME was not affected by the genotype of the DC vaccine, however, we observed that *Grm4*^{-/-} DC vaccination slightly decreased the frequency of TAMs and increased the frequency of neutrophils (Fig. 7H).

mGluR4 negatively regulates cAMP levels by suppressing the activity of AC. Forskolin is a potent AC agonist and is known to upregulate cAMP levels in DCs[17]. Forskolin is already used in clinics for the treatment of various diseases[51,52]. Considering our observations that forskolin upregulated the expression of costimulatory molecules in DCs (Fig. 6J), we postulated that forskolin could boost the efficacy of DC-based tumor vaccines. To test our hypothesis, DCs were pretreated with a commonly used concentration of forskolin before pulsing with
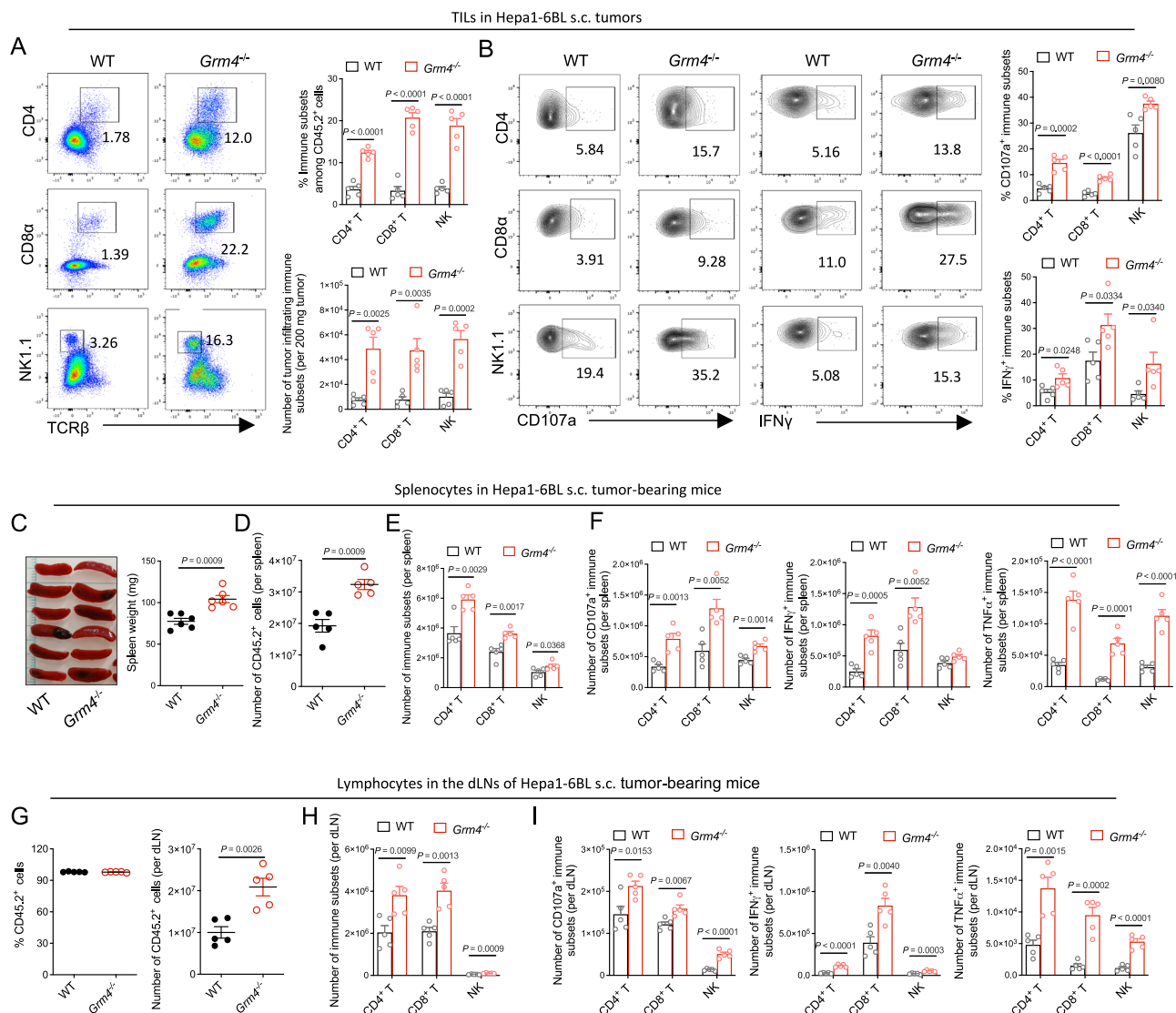
Fig. 5 | The infiltration and function of lymphocytes are promoted in tumors growing Grm4⁻/⁻ mice. A–I WT and *Grm4⁻/⁻* mice were s.c. injected with Hepa1-6BL (7×10^5) tumor cells. Mice were sacrificed on day 16. Tumor, spleen, and dLN single-cell suspensions were generated from the indicated groups of mice and stimulated with PMA/ionomycin plus protein transport inhibitors for 6 h before flow cytometry analysis. The infiltration of CD4⁺, CD8⁺ T, and NK cells and the expression of TNFα, CD107a, and IFNγ in WT and *Grm4⁻/⁻* mouse tumors were measured by flow cytometry. **A** The number of CD4⁺, CD8⁺ T, and NK cells and their proportion among CD45.2⁺ cells, and **B** CD107a⁺ and IFNγ⁺ CD4⁺, CD8⁺ T, and NK cells among the corresponding populations in Hepa1-6BL tumors growing in WT and *Grm4⁻/⁻* mice (*n* = 5 mice per group). **C** Representative spleen pictures and spleen weights

from mice bearing Hepa1-6BL tumors (*n* = 6 mice per group). **D** The number of CD45.2⁺ cells and **E** the indicated immune cell subsets in spleens (*n* = 5 mice per group). **F** The number of CD107a⁺, IFNγ⁺ and TNFα⁺ CD4⁺, CD8⁺ T, and NK cells among the corresponding cell subsets in spleens (*n* = 5 mice per group). **G** The percentage and number of live CD45.2⁺ cells, **H** the infiltration of CD4⁺, CD8⁺ T, and NK cells in dLNs (*n* = 5 mice per group). **I** The number of CD107a⁺, IFNγ⁺ and TNFα⁺ expressing CD4⁺, CD8⁺ T, and NK cells in dLNs of WT and *Grm4⁻/⁻* mouse bearing Hepa1-6BL tumors (*n* = 5 mice per group). Data were presented as mean ± SEM. Statistical significance was determined by unpaired *t*-test two-tailed (**A–I**). All biological experiments were repeated at least three times and yielded consistent results. Source data are provided as a Source Data file.

the tumor lysate. Vaccination with forskolin-treated DCs in a regimen similar to Fig. 7B effectively impeded the progression of orthotopic liver tumors (Fig. 7I). This indicates the potential of forskolin as a potent adjuvant of DC-based cancer vaccines.

mGluR4 signaling inhibits the maturation of human monocyte-derived DCs

Our finding revealed that mGluR4-mediated glutamatergic signaling negatively regulated the maturation and function of murine DCs. To further investigate the role of mGluR4 in human immune cells, we examined GRM4 expression across various immune cell subsets. We detected *GRM4* expression in CD4⁺ T, CD8⁺ T, and CD14⁺ monocytes

and CD14⁺ monocyte-derived dendritic cells (mo-DCs) and monocyte-derived macrophages (mo-Mac) from peripheral blood mononuclear cells (PBMCs) of healthy individuals (*n* = 5) (Fig. 8A). Consistent with our observations in mice, we found that human liver tumor cell HepG2-conditioned media (TCM) substantially upregulated the *GRM4* expression in human mo-DCs (Fig. 8B). Functionally, activation of mGluR4 with the selective agonist ADX88178 suppressed the expression of co-stimulatory molecules CD80 and CD86 in human mo-DCs. Conversely, pharmacological inhibition of mGluR4 signaling using UBP1112 and forskolin markedly enhanced the expression of these molecules. Furthermore, these treatments differentially affected the capacity of mo-DCs to stimulate T cell proliferation and IFNγ
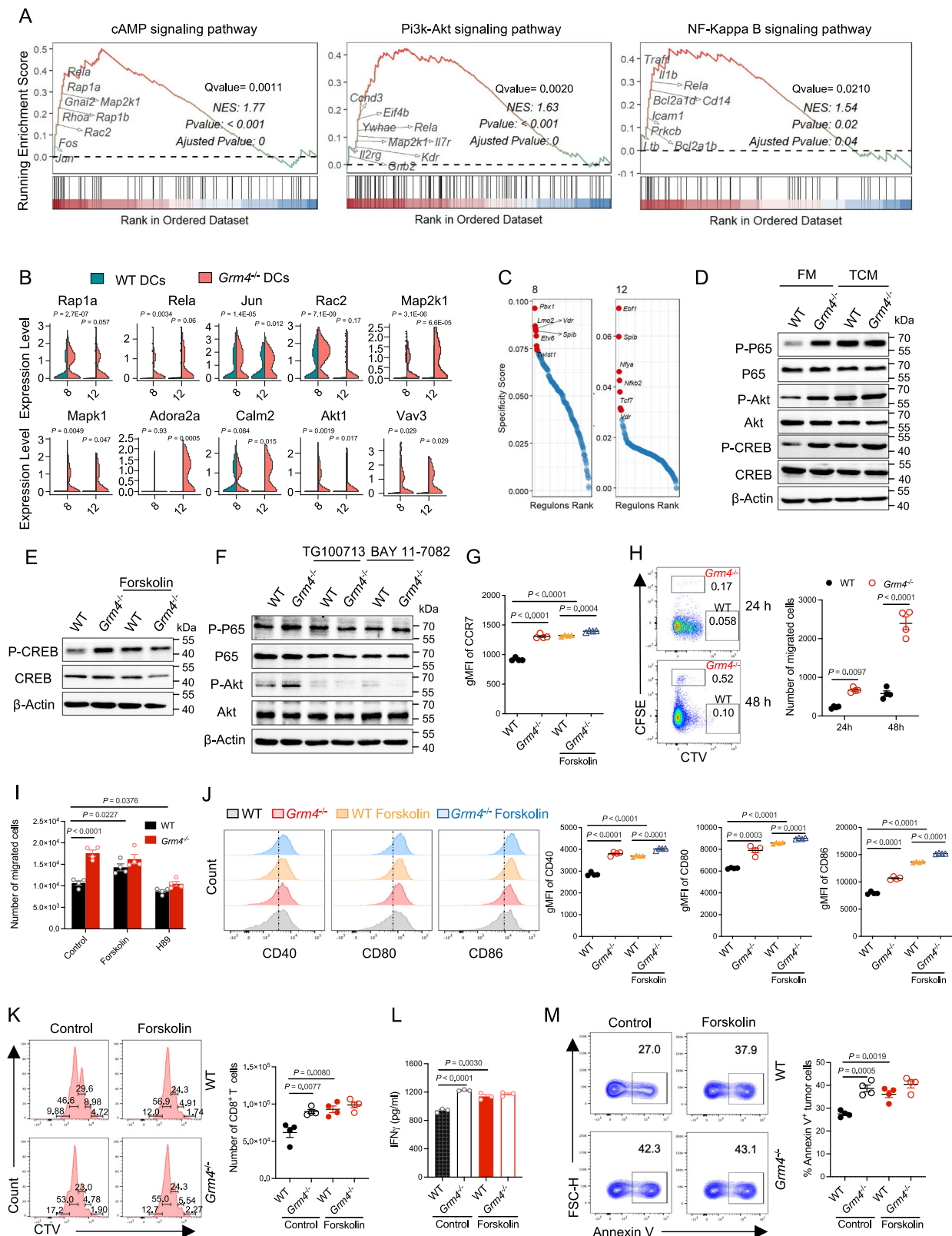
production, with mGluR4 activation reducing and inhibition enhancing this function (Fig. 8C–E). In contrast, treatment with ADX88178, UBP1112, and forskolin had minimal impact on the expression of costimulatory molecules in monocyte-derived macrophages or on the proliferative capacity of human CD8⁺ T cells (Fig. 8F–J). Collectively, these results underscore the critical role of mGluR4 signaling in modulating the maturation and functional activity of human mo-DCs.

Discussion

Mounting evidence indicates that the nervous system is anticipated as a critical regulator of cancer progression[12,15,53]. In the context of tumors, a triangular interaction between neurons, immune, and tumor cells is also emerging[54–57]. The neural-immune crosstalk can profoundly modulate the function of immune cells. In this study, we revealed the tumor-promoting role of the neurotransmitter glutamate receptor

Fig. 6 | mGluR4-mediated glutamatergic signaling suppresses the maturation and function of DCs. A The wave curve plots showing the core genes in the indicated signaling pathways in DCs from WT and *Grm4⁻/⁻* Hepa1-6BL tumor-bearing mice. Statistical differences were calculated by permutation test. The P-values were corrected with Benjamini-Hochberg adjustment. **B** Violin plots showing the expression of genes related to the signaling pathways as described in (**A**). **C** Rank plot of regulons in DCs from WT and *Grm4⁻/⁻* Hepa1-6BL tumor-bearing mice. **D–F** Total and phosphorylated protein levels of p65, Akt, and CREB in BMDCs after the indicated treatment were detected by Western Blot. **G** Expression of CCR7 in BMDCs after treatment with the AC agonist forskolin (10 μM) (*n* = 4 biological replicates). **H** Flow cytometric determination of BMDC migration in vivo (*n* = 4 mice per group). **I** Flow cytometric analysis of BMDC migration in vitro by transwell assay (*n* = 4 biological replicates). **J** Representative dot plots and gMFI of CD40, CD80, and CD86 in BMDCs after treatment with forskolin (10 μM) (*n* = 4 biological

replicates). **K–M** As described in the diagram in Fig. S14D, BMDCs were treated with forskolin (10 μM) for 24 h. Subsequently, cells were pulsed with OVA peptide before being co-cultured with CTV-labeled OT1 CD8⁺ T cells. **K** Representative histogram plots and statistical analysis of the proliferation of OT1 CD8⁺ T cells (*n* = 4 biological replicates). **L** The level of IFNγ in the cell culture supernatant was measured by ELISA kit (*n* = 3 biological replicates). **M** The apoptosis of Hepa1-6BL reflects the killing ability of CD8⁺ T cells by detecting the Annexin V⁺ cells (*n* = 4 biological replicates). Data were presented as mean ± SEM. Statistical significance was determined by student's *t*-test one-sided (**A, B**) corrected with Benjamini-Hochberg adjustment, student's *t*-test two-sided (**G, J, K, L, M**) and two-way ANOVA with Tukey's multiple comparisons test (**H, I**). All biological experiments were repeated at least three times and yielded consistent results. Source data are provided as a Source Data file.

mGluR4 by suppressing anti-tumor immunity. Deficiency of mGluR4 in mice effectively suppressed tumor growth and metastasis and prolonged tumor-bearing mouse survival by promoting DC maturation (Fig. 8K).

The nervous system can directly affect the development of osteosarcoma with high nerve infiltration[58,59]. Previously, the study has demonstrated that mGluR4 suppressed osteosarcoma[18], in which the nervous system might be involved. Our present study demonstrates that mGluR4 promoted tumor growth in various models. Given the important role of mGluR4 in the regulation of CNS, it is possible that the deficiency of mGluR4 altered the interaction between the nervous system and tumor cells or immune cells in the TME, leading to the suppression of tumor growth in vivo. Our bone marrow transfer experiment provided evidence that the expression of mGluR4 in the nervous system was not important for the mGluR4-mediated tumor progression, as transfer of WT BM into irradiated-*Grm4* deficient mice did not affect the tumor progression, at least in the tested tumor models. mGluR4 promoted tumor progression by suppressing immune responses because transferring *Grm4⁻/⁻* BM into irradiated WT mice was sufficient to suppress tumor growth to a similar level as in *Grm4⁻/⁻* mice. The effect of mGluR4 on the tumor is in line with the concept that the influences of the nervous system on the TME, immune responses, and immunotherapy can be independent of the receptor expression in neuron cells as immune cells directly respond to neurotransmitters and modulators[10,15,60,61]. Of note, it is possible that the nervous system can regulate mGluR4 expressing immune cells by releasing glutamate, impacting the immune response against tumors further.

Previous studies have reported that mGluR4 expression in tumor cells promotes tumor cell proliferation[62] and tumor development and is associated with poor prognosis in a variety of cancers, such as malignant neuroglioma[55], colorectal cancer[63], pediatric CNS tumors[64], rhabdomyosarcoma, and multiple myeloma[65]. Several studies have shown that mGluR4 expression is associated with good outcomes in patients with bladder and breast cancer and proposed that mGluR4-specific agonists control tumor progression, which is supported in immunodeficient mouse xenograft tumor models[66,67]. Although the regulation of mGluR4 on tumor cells has been well-studied, our understanding of the immunoregulatory role of mGluR4 is still very limited.

In this study, we evaluated the functional and mechanistic role of mGluR4 in a broader range of syngeneic tumor models. mGluR4 deficiency markedly curbed the growth of anti-PD-1 sensitive tumors (Hepa1-6BL[19], MCA1956[68] and MC38-OVA^dim s.c. tumors) and resistant tumors (SM1WT1[69]). The Hepa1-6BL orthotopic liver tumor burden and spontaneous lung metastases were also substantially suppressed in *Grm4⁻/⁻* mice, leading to substantially prolonged mouse survival. In addition, the experimental lung metastases of B16F10 and MC38 were noticeably decreased in mGluR4-deficient mice. Using bone marrow chimeras and neutralizing antibodies targeting IFNγ, CD8⁺ T, or NK

cells, we found that mGluR4 expression on immune cells impacted the tumor progression by regulating immune responses. Our study provides solid proof that mGluR4 promotes tumor immunoevasion.

This study is consistent with what was previously reported by Wan et al., that mGluR4 regulates the anti-tumor immunity in vivo[26]. In their study, the significant inhibition of tumor growth by genetic perturbation of mGluR4 was found in male mice only, and the number of tumor-infiltrating CD8⁺ T cells that produced IFNγ was lower in female compared to male B16 tumor-bearing mGluR4 KO mice. In our study, however, the tumor growth, immune cell infiltration, and function of mGluR4 were not affected by the gender of the mice and were reproducible across multiple tumor models. In addition, Wan et al. proposed that *Grm4⁻/⁻* CD8⁺ T cells showed a cell-intrinsic hyperproduction of IFNγ, while in our study, mGluR4 deficiency had little effect on the proliferation and production of effector molecules of isolated CD8⁺ T cells in vitro, but rather promoted the maturation and migration of dendritic cells. This is also supported by previous reports[17].

The expression of mGluR4 in different immune cell subsets was reported[17,18,21,26]. The expression of mGluR4 in CD4⁺ and CD8⁺ T cells, B cells, DCs, and macrophages was also confirmed in on mRNA level due to the lack of a commercially available specific anti-mGluR4 antibody. The differentiation and homeostasis of DC subsets were not affected by mGluR4 in naive mice. mGluR4 mainly regulated the maturation, function, and migration of cDC1, rather than cDC2 or pDC cells, although mGluR4 is expressed in all three DC subsets on a similar level. The reason for the preferential regulation of mGluR4 of cDC1 cells warrants further investigations in the future. In this study, we completely investigated the importance of mGluR4 in regulating DCs in the TME. mGluR4 exerted great influence on the infiltration and function of DCs, including DC migration, co-stimulatory molecule expression, antigen presentation, and cytokine production. *Grm4⁻/⁻* DCs from tumor tissues and LN were more potent in activating CD8⁺ T cells. Furthermore, the transfer of mGluR4-deficient DCs into tumor-bearing mice therapeutically suppressed liver tumor growth. This indicates that mGluR4 is a checkpoint of DC maturation, at least in the tumor settings.

The function of immune cells can be regulated by a range of neurotransmitters in the TME[10,15,60,61]. The binding of noradrenaline, released locally from sympathetic nerves or circulating catecholamines, to β2-adrenergic receptor (B2AR) expressed on myeloid-derived suppressor cell (MDSCs) and macrophages promoted immunosuppression[70,71]. Noradrenaline can directly limit CD8⁺ T cell function by promoting T cell exhaustion and infiltration of regulator T cells in the TME[72–74]. Likewise, nociceptor sensory nerves directly promote the exhaustion of cytotoxic T cells in the TME through the release of calcitonin gene-related peptide (CGRP)- a nociceptor-produced neuropeptide, which limits their capacity to eliminate melanoma[75]. B lymphocytes can generate gamma-aminobutyric acid (GABA) that binds to GABA_A receptors on CD8⁺ T cells and TAMs, leading to suppression of cytotoxic T cell responses and
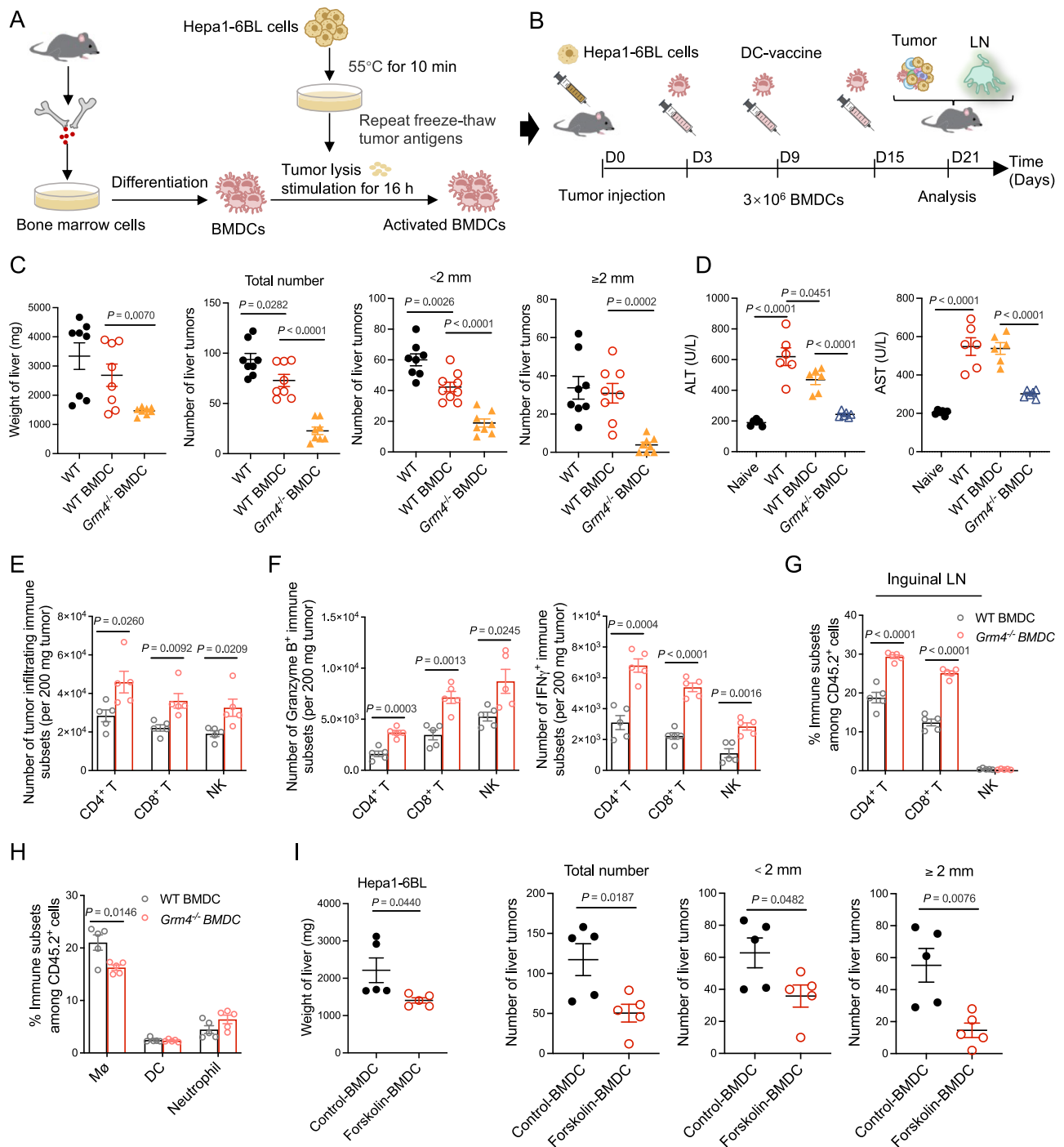
Fig. 7 | mGluR4 suppresses the anti-tumor efficacy of the DC-based tumor vaccine. A The schematic of the preparation of DC-based tumor vaccine. **B** Diagram of the therapeutic schedule of DC-based tumor vaccine in Hepa1-6BL tumor-bearing mice. Mice were sacrificed on day 21 and livers were collected for tumor burden quantification (**C, D**) or flow cytometry analysis (**E–H**). **C** Weights of livers, representative images of livers, and the number of liver tumor nodules with different sizes (*n* = 8 mice per group). **D** ALT and AST levels in serum of tumor-bearing mice from (**C**) on day 21 (*n* = 6 mice per group). **E** The number of CD4⁺, CD8⁺ T, and NK cells among CD45.2⁺ cells in Hepa1-6BL orthotopic liver tumors (*n* = 5 mice per group). **F** The number of granzyme B and IFNγ expressing lymphocytes amongst their corresponding subsets after the tumor single cell suspension was stimulated

with PMA/ionomycin plus protein transporter inhibitor for 6 h (*n* = 5 mice per group). **G** Frequency of CD4⁺ T, CD8⁺ T, and NK cells in the inguinal LN of Hepa1-6BL tumor-bearing mice (*n* = 5 mice per group). **H** The frequency of tumor-associated macrophages (TAM) and tumor-infiltrating DCs and neutrophil cells in Hepa1-6BL tumors (*n* = 5 mice per group). **I** Weights and the number of liver tumor with different sizes. Mice were intravenously injected with Hepa1-6BL tumor cell lysate-loaded WT BMDCs (3 × 10⁶) pretreated with forskolin (10 μM, 24 h) on days 3, 9 and 15 relatives to Hepa1-6BL tumor cell inoculation (*n* = 5 mice per group). Data were presented as mean ± SEM. Statistical significance was determined by unpaired *t*-test two-tailed (**C–I**). All biological experiments were repeated at least three times and yielded consistent results. Source data are provided as a Source Data file.
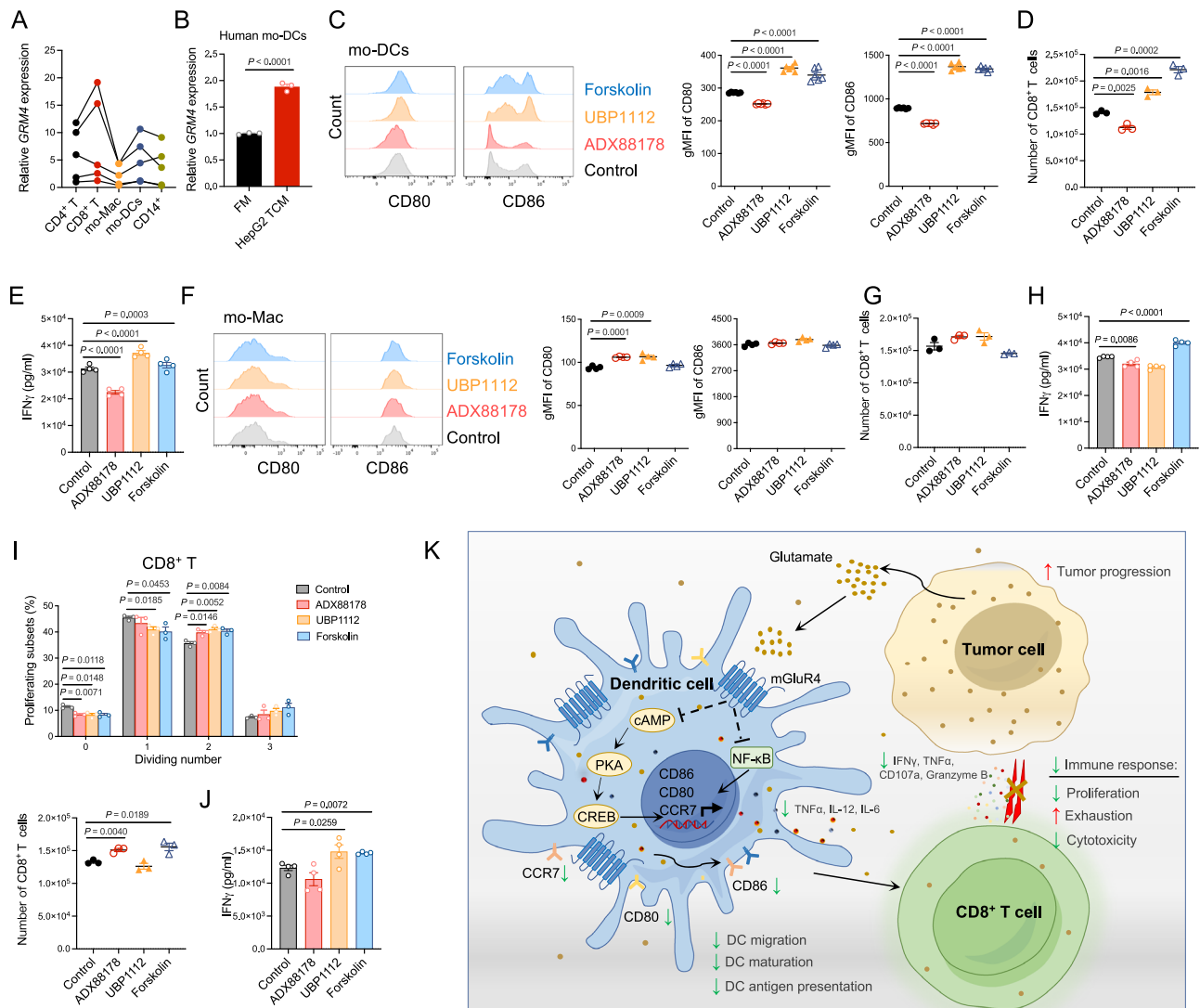
Fig. 8 | mGluR4-mediated glutamatergic signaling suppresses the function of human DCs. A The RNA level of mGluR4 in human CD4⁺ T, CD8⁺ T cells, CD14⁺ monocytes, mo-DCs, and mo-Mac cells was analyzed by qPCR analysis ($n = 5$ healthy donors). **B** Human mo-DCs were treated with FM or HepG2 TCM for 24 h. The expression of *GRM4* was determined ($n = 3$ biological replicates). **C–E** Human mo-DCs and (**F–H**) mo-Mac cells treated with ADX88178 (10 μM), UBP1112 (10 μM), or forskolin (10 μM) for 24 h were co-cultured with CTV-labeled human CD8⁺ T cells in the presence of anti-CD3 antibody (1 μg/ml) and IL-2 (100 U/ml) for 3 days. **C** The expression of CD80 and CD86 in mo-DCs ($n = 6$ biological replicates). **D** The total number of T cells ($n = 3$ biological replicates), and (**E**) the level of IFNγ in the cell culture supernatant ($n = 4$ biological replicates) after co-culture with mo-DCs. **F** The expression of CD80 and CD86 in mo-Mac cells ($n = 4$ biological replicates). (**G**) The

total number of T cells ($n = 3$ biological replicates), and (**H**) the level of IFNγ in the cell culture supernatant ($n = 4$ biological replicates) after co-culture with mo-Mac cells. **I** The proliferation and number of CD8⁺ T cells treated with ADX88178 (10 μM), UBP1112 (10 μM), or forskolin (10 μM) ($n = 3$ biological replicates) in the presence of anti-CD3 antibody (1 μg/ml), anti-CD28 antibody (1 μg/ml) and IL-2 (200 U/ml) for 3 days, and (**J**) the level of IFNγ in the cell culture supernatant ($n = 4$ biological replicates). **K** Schematic of mGluR4-mediated glutamatergic signaling in DCs in modulating anti-tumor immunity. Data were presented as mean ± SEM. Statistical significance was determined by an unpaired *t*-test two-tailed (**B–J**). All biological experiments were repeated at least three times. Source data are provided as a Source Data file.

an increased immune-suppressive state in TAMs, respectively[76]. In addition, platelet-derived peripheral serotonin directly upregulates tumor PD-L1 expression and suppresses T cell cytotoxic activity[77]. Recently, it has been reported that glutamate receptor N-methyl-D-aspartate receptor (NMDAR) is expressed in TAMs and promotes the immunosuppressive function of TAMs[19]. Our study shows that mGluR4 directly regulates DC maturation. To our knowledge, neurotransmitters acting as a direct checkpoint for DC maturation have not been reported so far.

ScRNA-seq and flow cytometric analysis revealed that mGluR4 deficiency profoundly influenced the immune signature of the TME. The tumor infiltration and function of CD4⁺ T, CD8⁺ T, and NK cells were increased in mGluR4 deficient mice in different tumor models. Of

interest, we observed an increased spleen size in tumor-bearing *Grm4⁻/⁻* mice, but not in naïve mice, correlating with an increased absolute number of CD4⁺, CD8⁺ T, and NK cells. Similar to the observations in the TME, mGluR4 deficient lymphocytes produced more IFNγ and showed a higher degranulation capacity in the spleens and dLNs of tumor-bearing *Grm4⁻/⁻* mice. This indicates that in the tumor setting, mGluR4 deficiency increased the immune responses systemically. Clinical and preclinical studies unravel the occurrence of systemic immune perturbations during tumor development as well as the crucial contribution of peripheral immune cells to an anti-tumor immune response[78]. The improved immune responses beyond the TME in *Grm4⁻/⁻* mice indicate the potential of mGluR4 as a tumor immunotherapy target.

Fallarino et al. reported the important role of mGluR4 in regulating cytokine production of DCs in the CNS in the EAE model[17]. mGluR4 can be activated by high concentrations of glutamate released from the neurons in the CNS, but little is known about the source and role of glutamate in the TME beyond the CNS. A key question is the source of glutamate in the TME and how tumors induce glutaminergic signaling. Previous studies showed a 20-fold increase in glutamate concentration in melanoma and colorectal tumor interstitial fluids (TIF)[29]. We found that glutamate concentration in the TIF and tumor lysate was significantly increased in the orthotopic liver tumors, which was 4-times higher than in the plasma and serum of tumor-bearing mice. Considering the high abundance of tumor cells relative to tumor-infiltrating immune cells in the TME, and the observation that tumor cells can produce significant amounts of glutamate, we reasoned that tumor cells represent the major source of glutamate in vivo. As such, this work contributes to previous literature that has implicated glutamate as an important mediator of immune suppression in the TME[19,29,79,80]. Although our data suggests that tumor-derived glutamate inhibits DC function and thus leads to tumor immunosuppression, other mechanisms may also lead to increased glutamate levels regulating immune progression. It has been reported that during maturation and antigen presentation, DCs release glutamate through the Xc-cystine/glutamate antiporter system, thereby impairing T cell proliferation[81]. This supports our work showing that glutamate is a major factor in regulating DC maturation during cancer progression. This demonstrates that glutamate inhibits the activation of DCs via the mGluR4 to limit tumor immune responses.

Adenyl cyclase is the key enzyme catalyzing the conversion of ATP to cAMP[82,83]. We and others[17] show that mGluR4 negatively regulated the activity of ACs and decreased the level of the second messenger cAMP in DCs. We found that forskolin-mediated AC activation diminished the negative regulation of mGluR4 on DC maturation and function to stimulate T cell proliferation and IFNγ production. PKA and exchange protein activated by cAMP (Epac) are the major cAMP effectors[82]. Garay et al., reported that activation of the cAMP/PKA pathway promotes the maturation of DCs, while activation of Epac negatively regulates the maturation and function of DCs[84]. In line with this report, our study shows that PKA inhibition by H89 treatment effectively decreased DC function and abolished the effects of mGluR4 on DCs. Altogether, these results show that mGluR4 negatively regulated DC maturation and function by suppressing the AC/cAMP/PKA pathway.

DCs are highly valued for their key role in anti-cancer vaccination therapies. More than 20 DC-based vaccines are currently in clinical trials in a variety of solid tumors, including melanoma, prostate cancer, glioma, and renal cell carcinoma[85–89]. Our study showed that the adoptive transfer of tumor-lysate pulsed $Grm4^{-/-}$ DCs significantly inhibited the progression of orthotopic liver tumors by increasing the expansion and infiltration of lymphocytes into the tumor tissue as well as enhancing their anti-tumor function. These observations further support our hypothesis that mGluR4-mediated glutamatergic signaling directly regulates murine DC function. Our data demonstrates that modulators of $Grm4$ can alter the phenotype and function of human DCs, underscoring the significant regulatory role of Grm4 in human DC biology. Given that optimal activation of DCs is essential for the efficacy of therapeutic tumor vaccines[48], our findings hold particular relevance. Pre-treatment of DCs with the clinical drug forskolin, which blocks mGluR4 downstream signaling pathway, enhanced the activation of both human and mouse DCs. Moreover, our forskolin-based vaccine therapy not only suppressed liver tumor progression in our models but also highlighted its promise for clinical translation.

The development of a specific anti-mGluR4 antibody or reporter mice would be useful to monitor mGluR4 expression at different stages of tumor development and its activity to regulate anti-tumor immunity. Of note, an uncommercial mGluR4 antagonist OptoGluNAM4.1 has been developed[90]. It will be interesting to assess its in vivo activity in the tumor setting in the future. Group III metabotropic glutamate receptors (mGluR4, mGluR6, mGluR7, mGluR8) exhibit high sequence homology and their expression has been documented in immune cells, including CD11c$^+$ cells[17]. While their expression in these cells is established, the extent of functional overlap and signaling interplay among these receptors in DCs remains unclear. Our current study focuses specifically on mGluR4, highlighting its role in DC regulation. However, the broader biological significance of the Group III mGluR family in immune modulation, particularly regarding receptor redundancy and compensatory mechanisms, warrants further investigation. Future studies should systematically analyze receptor expression profiles, cross-talk mechanisms, and functional relationships to clarify the therapeutic potential of targeting this receptor family in immune contexts. Tumor cells release various metabolites such as lactate to form an immunosuppressive TME. Recent studies showed that lactate limited the proinflammatory responses of DCs[91]. A previous study comparing the effect of different amino acids on DCs found glutamine to be the most important amino acid for DC development and function. In a tumor setting, tumor cells and cDC1s competed for glutamine[29]. From a different angle, we proved that the extracellular level of glutamate was increased in the TME, and glutamate was an important amino acid that suppressed DC maturation and function via mGluR4. This provides an insight into the importance of amino acids, especially glutamate as a signaling molecule to regulate anti-tumor responses. Supplementation of glutamine in diet suppressed tumor progression in preclinical tumor models, while glutamine could be converted into glutamate to tune anti-tumor immunity[29]. Our data supports the notion that supplementation of glutamine and blocking mGluR4-mediated glutamatergic signaling might be effective in enhancing anti-tumor immunity.

Our finding that mGluR4-mediated glutamatergic signaling suppressed the function of DCs provides an insight into the immunoregulation in the TME outside the CNS from the perspective that glutamate acts as a signaling molecule affecting anti-tumor immunity. The fact that $Grm4^{-/-}$ mice develop normally suggests that drugs blocking mGluR4 may be well tolerated and open the path for further studies validating our findings in a clinical setting.

Methods

Please see the Supporting information for more detailed materials and methods.

Cell lines and reagents

The mouse hepatocellular cell line Hepa1-6, Hepa1-6 derived cell line Hepa1-6BL, the colon cancer cell line MC38 and MC38-OVA^{dim}, the mouse melanoma cell lines B16F10 and SM1WT1, the fibrosarcoma cell line MCA1956 and the mouse connective tissue cell line L929 were cultured in DMEM supplemented with 10% fetal bovine serum (FBS, Umedium He Fei China), 100 U penicillin/ml and 100 μg/ml streptomycin at 37 °C in a humidified incubator under 95% air and 5% CO_2. The mouse macrophage cell line RAW264.7, the bone marrow-derived dendritic cell line DC2.4, the microglia cell line BV2, the bone marrow-derived dendritic cells (BMDCs), and the bone marrow-derived macrophage cells (BMDMs) were cultured in complete RPMI 1640 media. The generation of Hepa1-6BL cells referred to the study by Yuan et al.[19]. All cell lines were routinely tested for *Mycoplasma*, and cell line authentication was routinely performed.

The reagents and kits for biological assays are listed in Supplementary Tables 1, 2.

Mice

All animal experiments were carried out in accordance with the requirements of the Institutional Animal Care and Use Committee (IACUC) of Xuzhou Medical University (Approval No. 202209S041 and

202410T024). Adult C57BL/6 J wild-type (WT), *Grm4* knockout C57BL/6 J mice (*Grm4*^{-/-}) (Strain # S-KO-08619) and *Rag2*^{-/-} (Catalog # C001324) were purchased from Cyagen Biosciences, Inc. OT-I TCR-transgenic mice (The Jackson Laboratory, C57BL/6-Tg (TcraTcrb) 1100Mjb/J, Strain # 003831) were provided by Prof. Jing Yang (Xuzhou Medical University). All mice were genotyped using established protocols and used at 6 - 12 weeks of age. The animals were bred and maintained under specific pathogen-free (SPF) conditions, with ad libitum access to standard laboratory chow and water. Environmental parameters were strictly controlled: ambient temperature $22 \pm 2\,°C$, relative humidity 30-70%, and 12 h light/12 h dark cycle. Throughout the study, mice were randomly allocated to experimental groups. Both sexes were included with no significant sex-related differences observed in preliminary analyses. Euthanasia was performed via gradually increasing concentrations of CO_2 inhalation according to the ethical guidelines.

Generation of overexpression constructs
The recombinant pcDNA3.1-N-DYK-P2A eukaryotic expression vector containing mouse *Grm4* encoding was constructed by GenScript Biological Company.

Generation of CRISPR knockout constructs
The px459-Cas9-puro vector was digested with the *Bbs* I restriction enzyme to linearize the vector. CRISPR guides targeting exon 2 of murine *Grm*4 were designed (Supplementary Table 3). Forward and reverse oligos for each guide were annealed together with a standard annealing protocol, cloned into the px459-Cas9-puro vector by T4 ligation, amplified, and sequenced. DNA concentration was determined using a Nanodrop spectrophotometer.

Generation of *Grm*4 KO and OE DC2.4 cell lines
The DC2.4 cell line stably expressing *Grm4* was generated by lentiviral transduction of the parental cell line with the pCDH-CMV-Grm4-EF1-CopGFP-T2A-Puro construct. Expression of *Grm4* was confirmed using qPCR. The CRISPR-Cas9-mediated knockout of *Grm4* was generated by transient transfection of DC2.4 cells with the above-described constructs. Cells were treated with puromycin for selection, and the ablation of the target gene was confirmed by sequencing.

Animal tumor models
In a mouse subcutaneous tumor model, Hepa1-6BL (7×10^5), MC38-OVA[dim] (1×10^6), MCA1956 (1×10^6), or SM1WT1 (1×10^6) tumor cells with viability greater than 95% were injected subcutaneously (s.c.) into C57BL/6 WT or *Grm4*^{-/-} mice, respectively. Tumor measurements began on the 7th day and were taken every two days. Tumor sizes were determined by caliper square measurements and calculated as the product of two perpendicular diameters with data represented as mean ± SEM (mm²) for each group. Mice were sacrificed when the tumor grew to 100 mm², and the tumor tissue was collected and weighed.

In establishing the liver orthotopic model, Hepa1-6BL (5×10^5) cells were injected into WT or *Grm4*^{-/-} mice by tail vein with high pressure (hydrodynamic tail vein injection). Mice were sacrificed on day 21 relative to tumor cell inoculation and livers, lungs, and blood were collected. The whole liver tissue was weighed, and the orthotopic liver tumor burden and spontaneous lung metastatic burden were quantified by counting colonies on the surface of livers and lungs, respectively. For survival assays, Hepa1-6BL tumor cells with viability greater than 95% were injected tail vein with high pressure into C57BL/6 WT or *Grm4*^{-/-} mice. And mice were monitored for over 40 days.

For the lung metastasis model, MC38 (2×10^5), B16F10 (4×10^5) tumor cells were injected into the tail vein of WT or *Grm4*^{-/-} mice. The tumor mice were killed on day 15 or day 11 after the injection of MC38 or B16F10 tumor cells, and the tumor nodules on the surface of the lungs were counted.

For established tumor SM1WT1 experiments, mice were treated intraperitoneally (i.p.) with control Ig or anti-IFNγ (250 μg/mouse), anti-CD8β (100 μg/mouse) or Anti- asialoGM1 (ASGM1) (100 μg/mouse) on days -1, 0, 7, and 14 with the indicated doses, respectively.

BM transplantation and reconstitution
BM cells were obtained from the femurs of donor C57BL/6 WT mice and *Grm4*^{-/-} mice. Two doses of 5.5 Gy of whole-body irradiation were administered to recipient WT and *Grm4*^{-/-} mice at 4 h intervals. Recipient mice were injected intravenously with 5×10^6 BM cells/mouse after irradiation. Mice were provided with water containing neomycin for 4 weeks. Ten weeks after BM transplantation, mice were injected s.c. with MC38-OVA^{dim} tumor cells. Tumor growth was monitored by caliper square measurements. Mice were sacrificed when the tumor grew to 100 mm², and the tumor tissue was collected and weighed.

Generation of BM-derived macrophages and dendritic cells
Bone marrow (BM) cells were harvested from sex- and age-matched WT and *Grm4*^{-/-} littermates at 8 - 12 weeks of age. Then erythrocyte-depleted BM cells were cultured in complete RPMI 1640 media supplemented with 0.1% β-mercaptoethanol and 5% L929 cell supernatant for 4 days to generate BMDMs, or with 20 ng/ml murine granulocyte-macrophage colony-stimulating factor (GM-CSF) for 6-7 days to obtain inflammatory DCs (BMDC), or with 100 ng/ml FLT3L to generate a mixed population of type 1 conventional dendritic cells (cDC1), type 2 cDC (cDC2), and plasmacytoid dendritic cells (pDC) (FLT3L BMDC) for 7-9 days. FLT3L BMDC were sorted as cDC1s (MHCII^{+}CD11c^{+}CD24^{+}SIRPα^{-}B220^{-}) and cDC2s (MHCII^{+}CD11c^{+}CD24^{-}SIRPα^{+} B220^{-}) or pDCs (MHCII^{-}CD11c^{+}CD24^{-}SIRPα^{-}B220^{+}).

PBMCs isolation, mo-DCs and mo-Mac differentiation
Human peripheral blood mononuclear cells (PBMCs) were isolated from whole blood of five healthy donors by density centrifugation (Ficoll-Paque). CD14^{+} monocytes were purified from allogeneic PBMCs by magnetic separation, and mo-DCs were induced in RPMI 1640 complete medium with human GM-CSF (20 ng/ml) and IL-4 (10 ng/ml) for 7 days, and mo-Mac were induced in the presence of human M-CSF (50 ng/ml) for 5 days. At day 4, cells were refreshed with RPMI 1640 complete medium with respective cytokines.

Glutamate concentration determination
A total of 3×10^6 Hepa1-6BL cells, BMDCs, and BMDMs were cultured in 10 mm² dishes for 36 h, and cell culture supernatants were collected as tumor conditioned medium (TCM), BMDC conditioned medium (BMDC CM) and BMDM conditioned medium (BMDM CM). 3×10^6 Hepa1-6BL cells or BMDCs were collected, repeatedly freeze-thawed, and filtered as cell lysates. Plasma, serum, and tumor interstitial fluid (TIF) were collected as previously described[29]. In brief, orthotopic liver tumor tissues were cut into pieces and then mashed with a 70 μm strainer. The flow-through was collected as TIF, while single-cell precipitates were repeatedly freeze-thawed and filtered as tumor lysates. The matched blood was collected from the orbital venous plexus, and plasma and serum supernatant were collected after centrifugation. All the above-prepared samples were filtered by a 0.22 μm membrane aseptic filter and stored at -80 °C for later use. The concentration of glutamate was determined using a fluorometric assay kit according to the manufacturer's protocol.

Flow cytometry
Single-cell suspensions of mouse spleen, inguinal lymph node (iLN), thymus, liver, lung, BM, and tumor tissue were generated as previously described[19,28]. In brief, tissues were dissected from mice and then minced and digested in RPMI1640 containing 1 mg/ml Collagenase IV, 20 μg/ml DNase I, and 1% FBS for 35 min at 37 °C on a shaker. After digestion, the tissues were filtered through a 70 μm strainer and

resuspended in FACS buffer (1× PBS, 2% FBS) as a single-cell suspension. The ACK lysis buffer was performed for the lysis of red blood cells. The liver tissues were isolated by centrifugation on a 40 to 70% Percoll gradient to get mononuclear immune cells. The single-cell suspensions were incubated with antibodies blocking the Fc family of receptors for 20 min before the surface antibody staining. Zombie Aqua or 7AAD is used to distinguish dead cells, while Zombie Aqua is used for intracellular detection. For intracellular cytokine staining, cells were stained with surface antibodies as described above and then fixed and permeabilized with a Cytofix/Cytoperm™ Fixation/Permeabilization Solution Kit followed by staining with antibody. Cells were then collected on an Aria III flow cytometer or Canto II (BD Biosciences, NJ, USA) and performed using FlowJo v10 software (TreeStar Inc., USA). The information on flow cytometry antibodies used is listed in Supplementary Table 4. The gating strategies of flow cytometry data presented in this study can be found in Supplementary Figs. 9A, 10A, 12A, 16.

Sorting and culture of immune cell populations

For mouse immune cell populations, splenocytes were sorted as CD4⁺ T (CD45.2⁺TCRβ⁺CD4⁺), CD8⁺ T (CD45.2⁺TCRβ⁺CD8⁺), B (CD45.2⁺TCRβ⁻CD19⁺), CD11b⁺ (CD45.2⁺TCRβ⁻CD11b⁺), NK (CD45.2⁺TCRβ⁻NK1.1⁺), cDC1 (CD45.2⁺MHCII⁺CD11c⁺CD24⁺SIRPα⁻B220⁻), cDC2 (CD45.2⁺MHCII⁺CD11c⁺CD11b⁺SIRPα⁺CD24⁻B220⁻) or pDC (CD45.2⁺MHCII⁺CD11c⁺CD24⁻SIRPα⁻B220⁺) on an Aria III flow cytometer (BD Biosciences, NJ, USA). Sorted cells with purity over 95% were used in subsequent experiments. Hepa1-6BL tumors or iLN were harvested from WT and *Grm4⁻/⁻* mice at the end of the experiment, as described in the tumor model and flow cytometry section of the methods.

For human immune cell populations, PBMCs were isolated from whole blood of five healthy donors by density centrifugation (Ficoll-Paque). CD14⁺ monocytes were purified from allogeneic PBMCs by magnetic separation, and human CD4⁺ T (CD45.2⁺CD3⁺CD4⁺) and CD8⁺ T (CD45.2⁺CD3⁺CD8⁺) cells were isolated from PBMCs on an Aria III flow cytometer (BD Biosciences, NJ, USA).

T cell proliferation

CD4⁺ and CD8⁺ T cells were sorted from the spleens of WT or *Grm4⁻/⁻* naïve mice and then labeled with CellTrace Violet (CTV) according to the manufacturer's protocol. For CD4⁺ and CD8⁺ T cells proliferation, anti-CD3 antibody (1 μg/ml) was pre-packaged in 96-well plates for 2 h at 37 °C cell incubator before cells cultured for 3 days in RPMI 1640 supplemented with anti-CD28 antibody (1 μg/ml) and IL-2 (200 U/ml). Cell proliferation was determined by flow cytometry.

Human CD8⁺ T cells were labeled with CTV and then plated in a 96-well plate pre-coated with anti-CD3 antibody (1 μg/ml) for 2 h in the presence of anti-CD28 antibody (1 μg/ml) and human IL-2 (200 U/ml) for 3 days. T cell proliferation was determined by flow cytometry and the number was calculated based on the counting beads.

Macrophages or DCs and T cell coculture assay

Macrophages or DCs and T cell coculture assay were performed as previously described[19]. Briefly, macrophages or DCs (including BMDCs and sorted DCs from tumor and iLN tissue) were treated with different conditions according to the figure legends, pulsed with 1 ng/ml ovalbumin (OVA) peptide (SIINFEKL) for 2 h, and cocultured with CTV-labeled CD8⁺ T cells at the ratio of 1:10. Likewise, anti-CD3 antibody (1 μg/ml) and IL-2 (100 U/ml) were added to co-cultured CD4⁺ T cells and BMDCs. T cell proliferation was determined by flow cytometry, and IFNγ levels in the supernatant were measured with ELISA kits according to the manufacturer's instructions. Granzyme B and IFNγ expression were assessed by flow cytometry after PMA (0.8 μM) and ionomycin (1 μg/ml) stimulation in the presence of protein transport inhibitor Brefeldin A (10 μM) for 4 h. For CD8⁺ T-mediated killing activity, CD8⁺ T cells were collected and added to 5(6)-carboxyfluorescein diacetate succinimidyl ester (CFSE)-labeled Hepa1-6BL tumor cells at the ratio of 5:1 for 18 h. The killing ability of CD8⁺ T cells was analyzed by determining Annexin V⁺ Hepa1-6BL cells by flow cytometry.

Human PBMC mo-DCs and mo-Mac were treated with ADX88178, UBP1112 or forskolin for 24 h, followed by cocultured with CTV-labeled CD8⁺ T cells at a ratio of 1:10 with anti-CD3 antibody (1 μg/ml) and recombinant human IL-2 (100 U/ml) for 72 h.

Ex-vivo cytokine and degranulation by flow cytometry

Tumor single-cell suspensions were plated in a 96-well U-bottom plate (120 μl per well), suspended in complete RPMI 1640 medium containing 0.8 μM PMA / 1 μg/ml ionomycin plus 10 μM Brefildin A and anti-CD107a antibody for 6 h. Cells were stained for intracellular cytokine staining and analyzed using either the Aria III flow cytometer or Canto II instrument (BD Biosciences, NJ, USA).

ELISA

Supernatants from co-cultures of BMDCs or tumor-infiltrated DCs stimulated with 1 ng/ ml OVA peptide and CD8⁺ T cells for 2 days, were collected to quantify cytokine IFNγ release by ELISA according to the manufacturer's instructions. The level of mouse TNFα, IL-6, and IL-12 in the supernatant of DCs stimulated by LPS were determined using ELISA Kit according to the manufacturer's protocol.

Adoptive T cell transfer assay

Mouse spleens from WT or *Grm4⁻/⁻* mice were harvested. Spleens were mashed and lysed with ACK lysis buffer to remove red blood cells. Naïve CD4⁺ and CD8⁺ T cells were then sorted with anti-CD45.2, anti-TCRβ, and 7AAD antibodies by Aria III flow cytometer. WT or *Grm4⁻/⁻* T cells were injected i.v. into each *Rag2⁻/⁻* mice (4 to 6 weeks old) at a dose of 4 × 10⁶ per mouse and an orthotopic HCC model was performed 3 days after cell transfer. At the fifth and tenth days after the tumor model, naïve WT or *Grm4⁻/⁻* T cell subpopulations were sorted and adoptively transferred to the tumor-bearing *Rag2⁻/⁻* mice, respectively. The receipt mice were monitored and weighed every 5 days. After 21 days, mice were sacrificed, and liver tissues from mice were obtained for quantification.

Preparation of tumor cell lysate-pulsed DC vaccine

BMDCs were prepared as described above. For the tumor lysate preparation, Hepa1-6BL cells were collected and freeze-thawed six times (30 min at -80 °C, then thawed at 37 °C in a water bath). As described in Kumar et al.[49], tumor lysate was added to the BMDC cultures (approximately lysate from one tumor cell for each BMDC). Following 16 h of culture/pulsing with tumor lysates in the presence of a growth medium containing BMDCs, cells were harvested, thoroughly washed with sterile PBS, and resuspended in PBS.

Adoptive DC transfer assay

BMDCs were prepared from WT or *Grm4⁻/⁻* mice as described above[50]. Sensitized BMDCs (3 × 10⁶ cells) were washed twice with PBS, counted, and intravenously injected thrice (6−7 days apart) into each recipient WT Hepa1-6BL tumor-bearing mice. The receipt mice were monitored every four days and killed 21 days after tumor cell inoculation. The orthotopic liver tumor burden and spontaneous lung metastatic burden were quantified by counting colonies and analyzed for tumor-infiltrated immune cells.

Real-time PCR

Cells were harvested after treatment as indicated in the figure legends. Total RNA was isolated with TRIzol reagent and cDNA was further synthesized using Reverse Transcriptase Kit. The target genes were performed by quantitative real-time PCR using SYBR Green I Master Mix on a Light Cycler 480 system (Roche Group, BSL, CH). The specific

primer sets used in this study were designed according to their corresponding CDS regions and listed in Supplementary Table 5.

Western blotting

Cells were treated according to the instructions in the figure legends, washed with ice-cold PBS, and then lysed in RIPA lysis buffer. Equal amounts of protein lysates were performed using 8–10% SDS-polyacrylamide gels (SDS-PAGE) and transferred onto the PVDF membrane. The membranes were blocked with 5% BSA in PBST at room temperature for 2 h and incubated overnight with their respective primary antibodies (1:1000 dilutions) at 4 °C. Then membranes were washed four times with PBST and incubated with the corresponding HRP-conjugated secondary antibody (1:5000 dilutions) for 2 h at room temperature. The protein bands were visualized with enhanced chemiluminescence (ECL) on Quantity ONE software (Bio-rad, CA, USA). The primary antibodies used for WB are listed in Supplementary Table 4, and the uncropped and unprocessed scans of the most important blots are included in the Source Data file.

Glycolytic rate assay

The glycolytic rate assay was measured using a Seahorse XF96 Extracellular Flux Analyzer to assess glycolysis in cells. BMDCs (8×10^4) were plated into XFe96 cell culture microplates in 100 µl of growth media one day before the assay experiment and incubated at 37 °C with 5% CO_2, followed by treatment with FM or Hepa1-6BL TCM for 12 h. On the day of testing, BMDCs were washed with XF RPMI medium and cultured in this medium supplemented with 1 mM sodium pyruvate, 2 mM L-glutamine, and 10 mM glucose for 40 min at 37 °C in a humidified atmosphere without CO_2. For the glycolytic rate assay, 0.5 µM Rot/AA was added to port A, and 50 mM 2-DG was added to port B following the recommended concentrations. Glycolytic Rate Assay provides accurate measurements of glycolytic rates for basal conditions and compensatory glycolysis following mitochondrial inhibition.

ROS detection

BMDCs were plated at a density of 1×10^5 cells/well in a 48-well plate. BMDCs were treated with Hepa1-6BL TCM or not for 24 h. ROS levels were determined with CM-H2DCFDA. Briefly, BMDCs were washed and incubated in the presence of CM-H2DCFDA (10 µM) in cell culture media at 37 °C with 5% CO_2 for 30 min. After incubation, cells were washed and analyzed by flow cytometry within 2 h of staining.

Mitochondria membrane potential detection

BMDCs were seeded at a density of 1×10^5 cells/well in a 48-well plate. Cells were incubated for 24 h in the presence or absence of TCM, and then treated with CCP (10 µM) as a positive control for 20 min. Cells were washed and incubated with JC-1 for 20 min in the dark. The shift of fluorescence from red (JC-1 aggregates) to green (JC-1 monomers) was determined using flow cytometry to assess the mitochondria membrane potential.

ALT and AST detection in the serum

Blood samples were collected from orthotopic liver tumor mice for 21 days. Samples were kept at room temperature and separated by centrifugation at 600 g for 10 min. Serum aliquots were quantified of ALT and AST by Glutamic-pyruvic Transaminase (GPT) Activity Assay Kit and Micro Glutamic-oxalacetic Transaminase (GOT) Assay Kit, respectively. All the above biochemical parameters were detected according to the manufacturer's instructions.

Transwell migration assays

Migratory properties of immature BMDCs were investigated using 24-well transwell plates containing 8-mm-pore size polycarbonate filters (Corning, Life Science). WT or $Grm4^{-/-}$ BMDCs were added to the upper chamber (1×10^5 cells in a total volume of 100 µl), then CCL19 (50 ng/ml in a total volume of 600 µl) was added to the lower chamber, followed by incubation for 12 h at 37 °C. The number of migrated BMDC into the lower chamber was counted using BD CountBright absolute counting beads and immuno-phenotyped by FACS using the BD Canto II device. Moreover, the migrated cells at the bottom of the polycarbonate filter membrane were also counted under a light microscope.

DC migration in vivo

Immature BMDCs from $Grm4$-deficient or WT mice were labeled with CFSE or CTV in PBS, respectively. WT and $Grm4^{-/-}$ BMDCs were then mixed in equivalent proportions, and 1×10^6 cells were injected in the footpads of recipient mice 2 h before injection of E. coli (5×10^6 bacteria per footpad). At 24 h and 48 h after injection, popliteal lymph nodes (pLN) were extracted and prepared into a single-cell suspension[92]. Single-cell suspensions were analyzed by flow cytometry.

Single-cell RNA sequencing

Hepa1-6BL tumor tissues from $Grm4^{-/-}$ and WT mice (6 mice per group) were sampled, and single-cell suspensions were generated and stained as described by Yuan et al.[19]. CD45.2$^+$ cells were sorted on a FACS AriaIII. Around eight thousand cells for each sample were mixed with 10 × Genomics Chromium single-cell RNA master mix, followed by loading onto a 10 × Chromium chip according to the manufacturer's protocol to obtain single-cell cDNA. Libraries were subsequently prepared and sequenced using a NovaSeq sequencer (Illumina). Single-cell raw data were demultiplexed and converted to FASTQ format with Illumina bcl2fastq. The FASTQ data were processed with the Cell Ranger Single-Cell Software Suite Version 1.2 (https://support.10xgenomics.com/single-cell-gene-expression/software/pipelines/latest/what-is-cell-ranger) with default parameters according to the 10× Genomics guidelines, to align reads to the mouse reference genome (Ensembl_release106) and to further assign all reads to genes and individual cells based on the barcode information. Seurat v2.2.1 (3) was used to process the count data. The cells with less than 200 detected genes or > 5% mitochondrial transcripts were excluded. Expression data were normalized with the NormalizeData function, using the "LogNormalize" approach. Samples from $Grm4^{-/-}$ and WT mice were corrected with batch effects before combined analysis using "harmony" methods in the Seurat package in R v3.6.0. Clustering of cells based on gene expression was performed on all cells from both conditions with default parameters (function FindClusters), as well as a cluster-specific marker analysis (FindAllMarkers function), using only genes that were expressed at least in 25% of cells for each cluster. Different cell types were assigned to clusters based on known significant markers uniquely expressed in a particular cluster.

For each defined cluster/cell type, individual differential gene expression was analyzed between $Grm4^{-/-}$ and WT samples. The gene set enrichment analysis (GSEA) for each cell type was performed to identify significantly enriched functional pathways based on the differential gene list ranked by the log 2 FC between $Grm4^{-/-}$ and WT samples using the clusterProfiler package in R.

Activated regulons in each subset were analyzed using pySCENIC (Single Cell Regulatory Network Inference and Clustering) by Python (version) with raw count matrix as input. The regulons were identified by RcisTarget. Next, the regulon activity for each cell was scored by AUCell. The differentially activated regulons in each subset were identified by Wilcox. Test. The regulons with high AUCell score and their target genes were plotted by R.

Cell-cell interactions among the cell types were inferred through CellChat, a tool that can quantitatively infer and analyze intercellular communication networks from scRNA-seq data, delineating the specific signaling roles played by each cell type. The CellPhoneDB function

was used to compute the number and expression intensity of ligand-receptor pairs between cell types.

TCR repertoire analysis

Along with the single-cell RNA sequencing, the same samples were submitted to TCR repertoire analysis. The Single Cell V(D)J Reagent Kit protocol produces V(D)J enriched and 5′ gene expression Illumina-ready sequencing libraries. A library comprises standard Illumina paired-end constructs which begin and end with P5 and P7. For V(D)J enriched libraries, Read 1 encodes the 16 bp 10×™ Barcode, 10 bp UMI, and 13 bp Switch Oligo, as well as the 5′ end of an enriched transcript. For 5′ gene expression libraries, Read 1 encodes the 16 bp 10× Barcode and 10 bp UMI. Due to Enzymatic Fragmentation, for both libraries Read 2 encodes a random internal fragment of the corresponding insert. Sample index sequences are incorporated as the i7 index read. Chromium single-cell 5′ RNA-seq output was processed by Cell Ranger for V(D)J. Repertoire comparison analyses were visualized by R package scRepertoire for TCR diversity analysis and integrated analysis of scRNA-seq data and V(D)J-seq data. Repertoire comparison analyses were visualized by R package scRepertoire for TCR diversity analysis.

Statistics

Data entry and analyses were performed in a blinded fashion. Randomization was performed for in vivo experiments. Outliers were excluded from the analyses. All data points are from distinct samples. The precise sample number (n) was provided to indicate the number of biological samples in each experiment in the figure legends. Statistical analysis was performed using the GraphPad Prism software (Version 9.2) (P values are provided in the figures). Statistical significance was determined with the unpaired Student's t-test (two-tailed), Mann-Whitney test, one-way or two-way ANOVA with Tukey's or Sidak's multiple comparisons within multiple groups, survival curves were compared with the log-rank (Mantel–Cox) test. Data are shown as mean ± SEM unless otherwise indicated. $P < 0.05$ was considered significant. For scRNA-Seq analysis, transcriptome profile variations were determined by a NES obtained, using GSEA analysis. Statistical significance was determined with the Student's t-test (one-sided) and the P-values were corrected with Benjamini-Hochberg adjustment.

Reporting summary

Further information on research design is available in the Nature Portfolio Reporting Summary linked to this article.

Data availability

The RNA-seq data for mouse tumors generated in this study have been deposited in the Genome Sequence Archive (GSA) database under the accession code "CRA018231" (https://bigd.big.ac.cn/gsa/browse/CRA018231). All data generated or analyzed during this study are included in this manuscript and its Supplementary Information. Source data are provided with this paper.

References

1. Heras-Murillo, I., Adan-Barrientos, I., Galan, M., Wculek, S. K. & Sancho, D. Dendritic cells as orchestrators of anticancer immunity and immunotherapy. *Nat. Rev. Clin. Oncol.* **21**, 257–277 (2024).
2. Collin, M. & Bigley, V. Human dendritic cell subsets: an update. *Immunology* **154**, 3–20 (2018).
3. Merad, M., Sathe, P., Helft, J., Miller, J. & Mortha, A. The dendritic cell lineage: ontogeny and function of dendritic cells and their subsets in the steady state and the inflamed setting. *Annu Rev. Immunol.* **31**, 563–604 (2013).
4. Pittet, M. J., Di Pilato, M., Garris, C. & Mempel, T. R. Dendritic cells as shepherds of T cell immunity in cancer. *Immunity* **56**, 2218–2230 (2023).
5. Wculek, S. K., Cueto, F. J., Mujal, A. M., Melero, I., Krummel, M. F. & Sancho, D. Dendritic cells in cancer immunology and immunotherapy. *Nat. Rev. Immunol.* **20**, 7–24 (2020).
6. Garris, C. S. et al. Successful Anti-PD-1 Cancer immunotherapy requires T cell-dendritic cell crosstalk involving the cytokines IFN-gamma and IL-12. *Immunity* **55**, 1749 (2022).
7. Mondanelli, G. et al. A relay pathway between arginine and tryptophan metabolism confers immunosuppressive properties on dendritic cells. *Immunity* **46**, 233–244 (2017).
8. Oh, S. A. et al. PD-L1 expression by dendritic cells is a key regulator of T-cell immunity in cancer. *Nat. Cancer* **1**, 681–691 (2020).
9. Sabado, R. L., Balan, S. & Bhardwaj, N. Dendritic cell-based immunotherapy. *Cell Res* **27**, 74–95 (2017).
10. Hanahan, D. & Monje, M. Cancer hallmarks intersect with neuroscience in the tumor microenvironment. *Cancer Cell* **41**, 573–580 (2023).
11. Zahalka, A. H. & Frenette, P. S. Nerves in cancer. *Nat. Rev. Cancer* **20**, 143–157 (2020).
12. Winkler, F. et al. Cancer neuroscience: State of the field, emerging directions. *Cell* **186**, 1689–1707 (2023).
13. Schiller, M., Ben-Shaanan, T. L. & Rolls, A. Neuronal regulation of immunity: why, how and where?. *Nat. Rev. Immunol.* **21**, 20–36 (2021).
14. Pan, C. C. & Winkler, F. Insights and opportunities at the crossroads of cancer and neuroscience. *Nat. Cell Biol.* **24**, 1454–1460 (2022).
15. Mancusi, R. & Monje, M. The neuroscience of cancer. *Nature* **618**, 467–479 (2023).
16. Faulkner, S., Jobling, P., March, B., Jiang, C. C. & Hondermarck, H. Tumor neurobiology and the war of nerves in cancer. *Cancer Discov.* **9**, 702–710 (2019).
17. Fallarino, F. et al. Metabotropic glutamate receptor-4 modulates adaptive immunity and restrains neuroinflammation. *Nat. Med* **16**, 897–902 (2010).
18. Kansara, M. et al. Infiltrating myeloid cells drive osteosarcoma progression via GRM4 regulation of IL23. *Cancer Discov.* **9**, 1511–1519 (2019).
19. Yuan, D. et al. NMDAR antagonists suppress tumor progression by regulating tumor-associated macrophages. *Proc. Natl Acad. Sci. USA* **120**, e2302126120 (2023).
20. Zhang, Z. et al. Activation of metabotropic glutamate receptor 4 regulates proliferation and neural differentiation in neural stem/progenitor cells of the rat subventricular zone and increases phosphatase and tensin homolog protein expression. *J. Neurochem* **156**, 465–480 (2021).
21. Choi, W. M. et al. Metabotropic Glutamate receptor 5 in natural killer cells attenuates liver fibrosis by exerting cytotoxicity to activated stellate cells. *Hepatology* **74**, 2170–2185 (2021).
22. Reiner, A. & Levitz, J. Glutamatergic signaling in the central nervous system: Ionotropic and metabotropic receptors in concert. *Neuron* **98**, 1080–1098 (2018).
23. Wang, K., Zhao, J., He, M., Fowdur, M., Jiang, T. & Luo, S. Association of GRM4 gene polymorphisms with susceptibility and clinicopathological characteristics of osteosarcoma in Guangxi Chinese population. *Tumour Biol.* **37**, 1105–1112 (2016).
24. Jiang, C., Chen, H., Shao, L. & Dong, Y. GRM4 gene polymorphism is associated with susceptibility and prognosis of osteosarcoma in a Chinese Han population. *Med Oncol.* **31**, 50 (2014).
25. Koda, S. et al. The role of glutamate receptors in the regulation of the tumor microenvironment. *Front Immunol.* **14**, 1123841 (2023).
26. Wan, Z. et al. Targeting metabotropic glutamate receptor 4 for cancer immunotherapy. *Sci. Adv.* **7**, eabj4226 (2021).
27. Duong, E. et al. Type I interferon activates MHC class I-dressed CD11b(+) conventional dendritic cells to promote protective antitumor CD8(+) T cell immunity. *Immunity* **55**, 308–323 e309 (2022).

28. Wang, Y. et al. The transcription factor Zeb1 controls homeostasis and function of type 1 conventional dendritic cells. *Nat. Commun.* **14**, 6639 (2023).

29. Guo, C. et al. SLC38A2 and glutamine signalling in cDC1s dictate anti-tumour immunity. *Nature* **620**, 200–208 (2023).

30. Borcherding, N., Bormann, N. L. & Kraus, G. scRepertoire: An R-based toolkit for single-cell immune receptor analysis. *F1000Res* **9**, 47 (2020).

31. Valpione, S. et al. The T cell receptor repertoire of tumor infiltrating T cells is predictive and prognostic for cancer survival. *Nat. Commun.* **12**, 4098 (2021).

32. Valpione, S. et al. Immune-awakening revealed by peripheral T cell dynamics after one cycle of immunotherapy. *Nat. Cancer* **1**, 210–221 (2020).

33. Yan, J. et al. Control of metastases via myeloid CD39 and NK cell effector function. *Cancer Immunol. Res.* **8**, 356–367 (2020).

34. Yan, J. et al. Experimental lung metastases in mice are more effectively inhibited by blockade of IL23R than IL23. *Cancer Immunol. Res.* **6**, 978–987 (2018).

35. Mellman, I., Chen, D. S., Powles, T. & Turley, S. J. The cancer-immunity cycle: Indication, genotype, and immunotype. *Immunity* **56**, 2188–2205 (2023).

36. Niswender, C. M. & Conn, P. J. Metabotropic glutamate receptors: physiology, pharmacology, and disease. *Annu Rev. Pharm. Toxicol.* **50**, 295–322 (2010).

37. Habrian, C., Latorraca, N., Fu, Z. & Isacoff, E. Y. Homo- and hetero-dimeric subunit interactions set affinity and efficacy in metabotropic glutamate receptors. *Nat. Commun.* **14**, 8288 (2023).

38. Hu, Z. et al. Glycolysis drives STING signaling to facilitate dendritic cell antitumor function. *J. Clin. Invest.* **133**, e166031 (2023).

39. Hu, Z. et al. SENP3 senses oxidative stress to facilitate STING-dependent dendritic cell antitumor function. *Mol. Cell* **81**, 940–952 e945 (2021).

40. Kelly, B. & O'Neill, L. A. Metabolic reprogramming in macrophages and dendritic cells in innate immunity. *Cell Res.* **25**, 771–784 (2015).

41. Sayin, V. I., Ibrahim, M. X., Larsson, E., Nilsson, J. A., Lindahl, P. & Bergo, M. O. Antioxidants accelerate lung cancer progression in mice. *Sci. Transl. Med* **6**, 221ra215 (2014).

42. Anderson III, D. A., Dutertre, C. A., Ginhoux, F. & Murphy, K. M. Genetic models of human and mouse dendritic cell development and function. *Nat. Rev. Immunol.* **21**, 101–115 (2021).

43. Conn, P. J. & Pin, J. P. Pharmacology and functions of metabotropic glutamate receptors. *Annu Rev. Pharm. Toxicol.* **37**, 205–237 (1997).

44. Yin, S., Zamorano, R., Conn, P. J. & Niswender, C. M. Functional selectivity induced by mGlu(4) receptor positive allosteric modulation and concomitant activation of Gq coupled receptors. *Neuropharmacology* **66**, 122–132 (2013).

45. Fazio, F., Ulivieri, M., Volpi, C., Gargaro, M. & Fallarino, F. Targeting metabotropic glutamate receptors for the treatment of neuroinflammation. *Curr. Opin. Pharm.* **38**, 16–23 (2018).

46. Volpi, C. et al. Allosteric modulation of metabotropic glutamate receptor 4 activates IDO1-dependent, immunoregulatory signaling in dendritic cells. *Neuropharmacology* **102**, 59–71 (2016).

47. Deka, A. et al. Non-canonical NF-κB signaling limits the tolerogenic β-catenin-Raldh2 axis in gut dendritic cells to exacerbate intestinal pathologies. *Embo j.* **43**, 3895–3915 (2024).

48. Saxena, M., van der Burg, S. H., Melief, C. J. M. & Bhardwaj, N. Therapeutic cancer vaccines. *Nat. Rev. Cancer* **21**, 360–378 (2021).

49. Kumar, A. et al. Dendritic cell therapy augments antitumor immunity triggered by CDK4/6 inhibition and immune checkpoint blockade by unleashing systemic CD4 T-cell responses. *J. Immunother. Cancer* **11**, e006019 (2023).

50. Lutz, M. B. et al. An advanced culture method for generating large quantities of highly pure dendritic cells from mouse bone marrow. *J. Immunol. Methods* **223**, 77–92 (1999).

51. Sapio, L. et al. The natural cAMP elevating compound forskolin in cancer therapy: Is it time?. *J. Cell Physiol.* **232**, 922–927 (2017).

52. Roshni, P. T. & Rekha, P. D. Biotechnological interventions for the production of forskolin, an active compound from the medicinal plant, Coleus forskohlii. *Physiol. Mol. Biol. Plants* **30**, 213–226 (2024).

53. Monje, M. et al. Roadmap for the emerging field of cancer neuroscience. *Cell* **181**, 219–222 (2020).

54. Venkataramani, V. et al. Glutamatergic synaptic input to glioma cells drives brain tumour progression. *Nature* **573**, 532–538 (2019).

55. Takano, T., Lin, J. H., Arcuino, G., Gao, Q., Yang, J. & Nedergaard, M. Glutamate release promotes growth of malignant gliomas. *Nat. Med.* **7**, 1010–1015 (2001).

56. Long, Y. et al. Dysregulation of glutamate transport enhances treg function that promotes VEGF blockade resistance in glioblastoma. *Cancer Res.* **80**, 499–509 (2020).

57. Namkoong, J. et al. Metabotropic glutamate receptor 1 and glutamate signaling in human melanoma. *Cancer Res* **67**, 2298–2305 (2007).

58. Zheng, X. Q., Wu, Y. H., Huang, J. F. & Wu, A. M. Neurophysiological mechanisms of cancer-induced bone pain. *J. Adv. Res.* **35**, 117–127 (2022).

59. Wan, Q. Q. et al. Crosstalk between bone and nerves within bone. *Adv. Sci. (Weinh.)* **8**, 2003390 (2021).

60. Jiang, S. H. et al. GABRP regulates chemokine signalling, macrophage recruitment and tumour progression in pancreatic cancer through tuning KCNN4-mediated Ca(2+) signalling in a GABA-independent manner. *Gut* **68**, 1994–2006 (2019).

61. Qiao, G., Chen, M., Bucsek, M. J., Repasky, E. A. & Hylander, B. L. Adrenergic Signaling: A Targetable Checkpoint Limiting Development of the Antitumor Immune Response. *Front Immunol.* **9**, 164 (2018).

62. Luksch, H. et al. Silencing of selected glutamate receptor subunits modulates cancer growth. *Anticancer Res* **31**, 3181–3192 (2011).

63. Chang, H. J., Yoo, B. C., Lim, S. B., Jeong, S. Y., Kim, W. H. & Park, J. G. Metabotropic glutamate receptor 4 expression in colorectal carcinoma and its prognostic significance. *Clin. Cancer Res.* **11**, 3288–3295 (2005).

64. Brocke, K. S. et al. Glutamate receptors in pediatric tumors of the central nervous system. *Cancer Biol. Ther.* **9**, 455–468 (2010).

65. Stepulak, A. et al. Expression of glutamate receptor subunits in human cancers. *Histochem Cell Biol.* **132**, 435–445 (2009).

66. Xiao, B. et al. Glutamate metabotropic receptor 4 (GRM4) inhibits cell proliferation, migration and invasion in breast cancer and is regulated by miR-328-3p and miR-370-3p. *BMC Cancer* **19**, 891 (2019).

67. Zhang, H. et al. The role of NK cells and CD39 in the immunological control of tumor metastases. *Oncoimmunology* **8**, e1593809 (2019).

68. Molgora, M. et al. TREM2 modulation remodels the tumor myeloid landscape enhancing anti-PD-1 Immunotherapy. *Cell* **182**, 886–900 e817 (2020).

69. Knight, D. A. et al. Host immunity contributes to the anti-melanoma activity of BRAF inhibitors. *J. Clin. Invest* **123**, 1371–1381 (2013).

70. Mohammadpour, H. et al. β2 adrenergic receptor-mediated signaling regulates the immunosuppressive potential of myeloid-derived suppressor cells. *J. Clin. Invest* **129**, 5537–5552 (2019).

71. Sloan, E. K. et al. The sympathetic nervous system induces a metastatic switch in primary breast cancer. *Cancer Res.* **70**, 7042–7052 (2010).

72. Nakai, A., Hayano, Y., Furuta, F., Noda, M. & Suzuki, K. Control of lymphocyte egress from lymph nodes through β2-adrenergic receptors. *J. Exp. Med.* **211**, 2583–2598 (2014).

73. Qiao, G. et al. β-Adrenergic signaling blocks murine CD8(+) T-cell metabolic reprogramming during activation: a mechanism for

immunosuppression by adrenergic stress. *Cancer Immunol. Immunother.* **68**, 11–22 (2019).

74. Kamiya, A. et al. Genetic manipulation of autonomic nerve fiber innervation and activity and its effect on breast cancer progression. *Nat. Neurosci.* **22**, 1289–1305 (2019).

75. Balood, M. et al. Nociceptor neurons affect cancer immuno-surveillance. *Nature* **611**, 405–412 (2022).

76. Zhang, B. et al. B cell-derived GABA elicits IL-10(+) macrophages to limit anti-tumour immunity. *Nature* **599**, 471–476 (2021).

77. Schneider, M. A. et al. Attenuation of peripheral serotonin inhibits tumor growth and enhances immune checkpoint blockade therapy in murine tumor models. *Sci. Transl. Med.* **13**, eabc8188 (2021).

78. Hiam-Galvez, K. J., Allen, B. M. & Spitzer, M. H. Systemic immunity in cancer. *Nat. Rev. Cancer* **21**, 345–359 (2021).

79. Sharma, M. K., Seidlitz, E. P. & Singh, G. Cancer cells release glutamate via the cystine/glutamate antiporter. *Biochem Biophys. Res Commun.* **391**, 91–95 (2010).

80. Ye, Z. C. & Sontheimer, H. Glioma cells release excitotoxic concentrations of glutamate. *Cancer Res.* **59**, 4383–4391 (1999).

81. Pacheco, R. et al. Glutamate released by dendritic cells as a novel modulator of T cell activation. *J. Immunol.* **177**, 6695–6704 (2006).

82. Maurice, D. H., Ke, H., Ahmad, F., Wang, Y., Chung, J. & Manganiello, V. C. Advances in targeting cyclic nucleotide phosphodiesterases. *Nat. Rev. Drug Discov.* **13**, 290–314 (2014).

83. Schuster, D., Khanppnavar, B., Kantarci, I., Mehta, V. & Korkhov, V. M. Structural insights into membrane adenylyl cyclases, initiators of cAMP signaling. *Trends Biochem Sci.* **49**, 156–168 (2024).

84. Garay, J. et al. Crosstalk between PKA and Epac regulates the phenotypic maturation and function of human dendritic cells. *J. Immunol.* **185**, 3227–3238 (2010).

85. Ge, C. et al. Phase I clinical trial of a novel autologous modified-DC vaccine in patients with resected NSCLC. *BMC Cancer* **17**, 884 (2017).

86. Lee, J. M. et al. Phase I Trial of Intratumoral Injection of CCL21 gene-modified dendritic cells in lung cancer elicits tumor-specific immune responses and CD8(+) T-cell Infiltration. *Clin. Cancer Res.* **23**, 4556–4568 (2017).

87. Erhart, F. et al. Immunological analysis of phase II glioblastoma dendritic cell vaccine (Audencel) trial: immune system characteristics influence outcome and Audencel up-regulates Th1-related immunovariables. *Acta Neuropathol. Commun.* **6**, 135 (2018).

88. Wen, P. Y. et al. A randomized double-blind placebo-controlled phase II trial of dendritic cell vaccine ICT-107 in newly diagnosed patients with glioblastoma. *Clin. Cancer Res.* **25**, 5799–5807 (2019).

89. Boudewijns, S. et al. Autologous monocyte-derived DC vaccination combined with cisplatin in stage III and IV melanoma patients: a prospective, randomized phase 2 trial. *Cancer Immunol. Immunother.* **69**, 477–488 (2020).

90. Rovira, X. et al. OptoGluNAM4.1, a photoswitchable allosteric antagonist for real-time control of mGlu4 receptor activity. *Cell Chem. Biol.* **23**, 929–934 (2016).

91. Sanmarco, L. M. et al. Lactate limits CNS autoimmunity by stabilizing HIF-1alpha in dendritic cells. *Nature* **620**, 881–889 (2023).

92. Barbet, G. et al. The calcium-activated nonselective cation channel TRPM4 is essential for the migration but not the maturation of dendritic cells. *Nat. Immunol.* **9**, 1148–1156 (2008).

Acknowledgements

Author contributions

J.Y., X.J., and J.H. conceptualized and designed this study. X.J., J.H., Y.L., D.Y., and G.S. performed and analyzed most of the experiments. X.J., J.H., B.D., C.T., Y.L., D.Y., G.S., Z.F., and S.S. participated in the collection of samples, reporting data, organizing data, constructing the databases, and scoring of mice. J.Y., X.J. and J.H. wrote the draft manuscript, and J.Y., X.J., J.H., E.-M.P., and S.K. reviewed the manuscript. J.Y. supervised the project. All authors approved the study and revised the manuscript.

Competing interests

The authors declare no competing interests.

Additional information

Supplementary information The online version contains supplementary material available at https://doi.org/10.1038/s41467-025-60922-y.

Correspondence and requests for materials should be addressed to Chunrong Tong, Biping Deng, Jing Hu or Juming Yan.

Peer review information *Nature Communications* thanks Byungsuk Kwon and the other, anonymous, reviewer(s) for their contribution to the peer review of this work. A peer review file is available

Reprints and permissions information is available at http://www.nature.com/reprints

Publisher's note Springer Nature remains neutral with regard to jurisdictional claims in published maps and institutional affiliations.